Fe^{II} in Different Macrocycles: Electronic Structures and Properties

Meng-Sheng Liao, John D. Watts, and Ming-Ju Huang*

Department of Chemistry, P.O. Box 17910, Jackson State University, Jackson, Mississippi 39217

Received: May 2, 2005; In Final Form: July 7, 2005

A theoretical comparative study of complexes of porphyrin (P), porphyrazine (Pz), phthalocyanine (Pc), porphycene (Pn), dibenzoporphycene (DBPn), and hemiporphyrazine (HPz) with iron (Fe) has been carried out using a density functional theory (DFT) method. The difference in the core size and shape of the macrocycle has a substantial effect on the electronic structure and properties of the overall system. The ground states of FeP and FePc were identified to be the $^3A_{2g}$ $[(d_{xy})^2(d_{z^2})^2(d_\pi)^2]$ state, followed by ^3E_g $[(d_{xy})^2(d_{z^2})^1(d_\pi)^3]$. For FePz, however, the $^3E_g-{}^3A_{2g}$ energy gap of 0.02 eV may be too small to distinguish between the ground and excited states. When the symmetry of the macrocycle is reduced from D_{4h} to D_{2h}, the degeneracy of the d_π (d_{xz}, d_{yz}) orbitals is removed, and the ground state becomes $^3B_{2g}$ $[(d_{xy})^2(d_{z^2})^1(d_{yz})^2(d_{xz})^1]$ or $^3B_{3g}$ $[\cdots(d_{yz})^1(d_{xz})^2]$ for FePn, FeDBPn, and FeHPz. The calculations also show how the change of the macrocycle can influence the axial ligand coordination of pyridine (Py) and CO to the Fe^{II} complexes. Finally, the electronic structures of the mono- and dipositive and -negative ions for all the unligated and ligated iron macrocycles were elucidated, which is important for understanding the redox properties of these compounds. The differences in the observed electrochemical (oxidation and reduction) properties between metal porphycenes (MPn) and metal porphyrins (MP) can be accounted for by the calculated results (orbital energy level diagrams, ionization potentials, and electron affinities).

1. Introduction

Metal complexes with various macrocycles, such as porphyrins (Ps), phthalocyanines (Pcs), and their analogues, have attracted considerable interest because of their biological significance, catalytic properties, and potential technological applications. Metal porphyrins (MPs) are well-known for their biological functions such as photosynthesis, respiration, and electron transport.[1] Metal phthalocyanines (MPcs) have found numerous applications in industry.[2] For these reasons, recent decades have witnessed an explosion of experimental studies on MPs and MPcs. On the other hand, a large number of related, interesting compounds have been synthesized and characterized in the past and recent years.[3−26] As basic units of many proteins and enzymes of hemoproteins, iron porphyrins have been the subject of intense experimental as well as theoretical investigations. Since the partial occupancy of the 3d shell can yield a number of low-lying electronic states that are within a narrow energy range, there was a long-term debate as to what is the ground state for unligated, four-coordinated Fe^{II} porphyrins (FePs). From available experimental data, there seems to be little doubt that FePs exist in an intermediate-spin ($S = 1$) state, due in part to the high energy of the antibonding b_{1g} ($d_{x^2-y^2}$) orbital which leaves it unoccupied. Among the four possible intermediate-spin states, only $^3A_{2g}$, arising from the $(d_{xy})^2(d_{z^2})^2(d_\pi)^2$ configuration, is compatible with Mössbauer, magnetic, and proton NMR data.[27,28] Calculations[29] using the ADF program (see section 2) support these experimental assignments. A comparison of the results on FeP from different computational methods is reported in the Supporting Information. The success of ADF calculations on iron porphyrins lends confidence in applying the same program to other iron complexes.

Without axial ligation, the ground state of Fe^{II} in a macrocycle depends mainly on the nature of the macrocycle. This theoretical study serves to underscore how some changes in ligand size, shape, and structure can have an important effect on the electronic state and properties of various Fe^{II} macrocycles. In addition to porphyrin, the macrocycles considered here, illustrated in Figure 1, include porphyrazine (Pz), phthalocyanine (Pc), porphycene (Pn), dibenzoporphycene (DBPn), and hemiporphyrazine (HPz), thereby extending the previous work.[30] The three latter macrocycles were selected because they are quite symmetric and display properties analogous to, or rather different from, those of the porphyrins/phthalocyanines. An iron porphycene, FeTPrPn (iron tetra-*n*-propylporphycene), has been characterized in an intermediate-spin ($S = 1$) state by means of ^1H NMR spectroscopy,[25a,b] but the details of its electronic configuration are unknown. Except for FeP and FePc, no experimental information is available about the precise electronic structure of the other Fe^{II} macrocycles,

Pz is isoelectronic with P, where the four methine bridge carbon atoms are replaced by nitrogen atoms, and the meso H atoms are absent. An important difference between the aza N atom and the methine bridge is the higher electronegativity of the former. Pc can be regarded as a derivative of Pz, where the aromatic system is enlarged by adding four benzo rings. There have been theoretical comparative studies of MP, MPz, and MPc with M = Ni[31] and Zn.[32] But these studies mainly involved interpretation of the absorption spectra of the metal complexes.

Pn is a constitutional isomer of P; the former contains a rectangular inward-pointing N_4 coordinating core, featuring two $(CH)_2$ linkages between the pyrrole rings. A number of spectral and electrochemical studies have been carried out on porphycenes and their metal derivatives (e.g., refs 6−21); they have revealed noticeable differences in physical and chemical properties between the two kinds of tetrapyrrole macrocycles. There have been DFT[33,34] and second-order Møller−Plesset (MP2)[34] calculations on free-base porphycene (H_2Pn), but theoretical

* Corresponding author. Email: mhuang@chem.jsums.edu.

10.1021/jp0581476 CCC: $30.25
Published on Web 08/13/2005

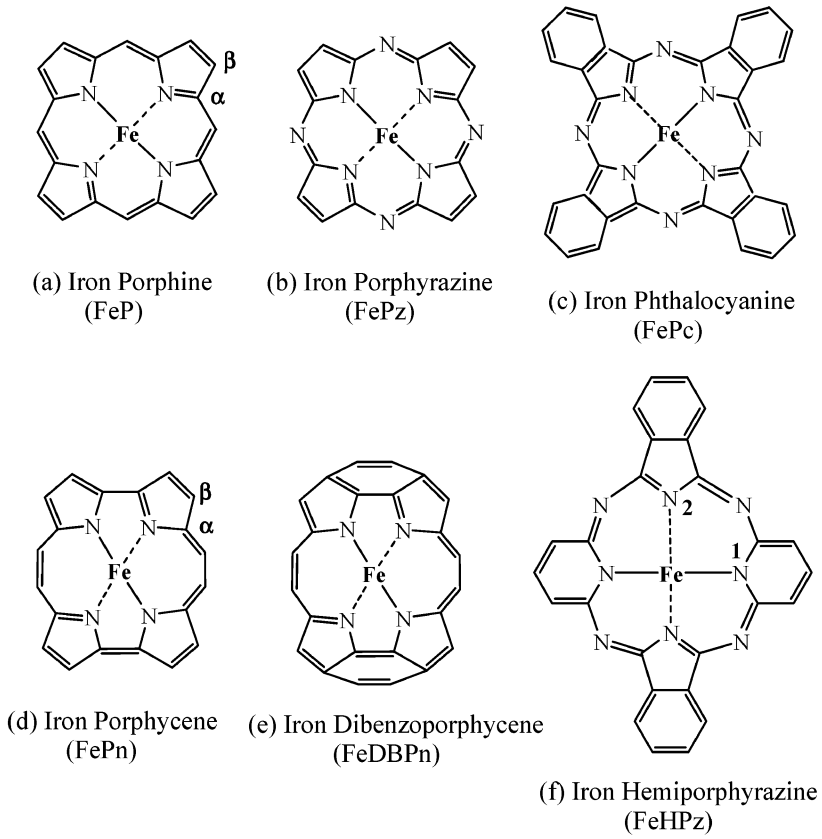

Figure 1. Molecular structures of the various iron macrocycles.

studies of some MPns (M = Ni, Sn) were limited mainly to semiempirical methods.[35]

DBPn is an expanded Pn, having two conjugated six-membered rings (benzo rings) which are formed by bridging the pyrrole β-carbons of adjacent pyrrole rings. Several substituted DBPn compounds have been synthesized.[22] UV−vis spectra[22] and theoretical calculations[36] on free-base molecules show some marked difference in the electronic structures between Pn and DBPn. The expanded porphycene also allows metal coordination,[15] but no theoretical studies of MDBPns have been reported.

HPz is a phthalocyanine-like macrocycle, resulting when two opposite isoindoles in Pc are replaced by two pyridines. The HPz macrocycle exhibits some interesting properties,[3−5] because the four-coordinating nitrogens are not equivalent. Several experimental studies have been carried out on the HPz complexes with first-series transition metals.[5] Theoretical work has mainly been concerned with free-base H_2HPz so far.[37]

One of the most important phenomena in metal macrocycles is the coordination of the central metal to molecules in addition to the macrocycle. Iron macrocycles exhibit particularly strong attraction for additional ligands, to which their electronic structures are sensitive. Another purpose of this paper is to examine how the differences in macrocycle affect the axial ligation properties of the Fe^{II} complexes using pyridine (Py) and carbonyl (CO) as the axial ligand.

2. Computational Method

All calculations were carried out using the Amsterdam Density Functional (ADF) program package (version 2.0.1) developed by Baerends and co-workers.[38] Triple-ζ Slater-type orbitals (STOs) basis sets were employed for the Fe 3s/3p/3d/4s, the C/N/O 2s/2p, and the H 1s valence shells. Single-ζ STOs were used for core orthogonalization. Polarization functions were added to the valence bases: one p-type polarization function for Fe and H and one d-type polarization function for C/N/O. The other shells of lower energy, i.e., [Ne] for Fe and [He] for C/N/O, are considered as core shells and kept frozen according to the frozen-core technique.[38] The exchange-correlation potential used is based on the density-parametrized form of Vosko, Wilk, and Nusair.[39] Nonlocal corrections are based on Becke's gradient functional for exchange[40] and Perdew's gradient functional for correlation[41] and were treated by a fully self-consistent method. Relativistic corrections of the valence electrons were calculated using the quasi-relativistic method of Ziegler, Baerends, et al.[42] For the open-shell states, the unrestricted Kohn−Sham (UKS) spin-density functional approach was adopted. The UKS equation is the analogue of the unrestricted Hartree−Fock (UHF) equation; the N-particle wave function is a single determinant and not necessarily an eigenfunction of the spin operator S^2. There is no implementation of an evaluation of $|S^2|$ in the present ADF program used, and hence, spin contamination could not be assessed here.

3. Results and Discussion

The molecular structures of the various iron macrocycles are illustrated in Figure 1. For computational economy, the calculations were carried out for the unsubstituted macrocycles. The systems that have been synthesized contain various different substituent groups (methyl, vinyl, phenyl, ethyl, etc.) at the periphery of the ring. Previous calculations[29] showed that many of the electronic properties are insensitive to the nature of these peripheral substituents. The MP, MPz, and MPc molecules in Figure 1 have D_{4h} symmetry, as established by experiment and calculation.[32] Taking the z-axis as perpendicular to the macrocycle, the five metal 3d orbitals transform as a_{1g} (d_{z^2}), b_{1g} ($d_{x^2-y^2}$),

TABLE 1: Calculated Relative Energies (*E*, eV) for Different Configurations in FeP, FePz, and FePc

configuration[a]					*E* (R)[b]		
b_{2g}/d_{xy}	a_{1g}/d_{z^2}	$1e_g/d_\pi$	$b_{1g}/d_{x^2-y^2}$	state	FeP	FePz	FePc
2	2	2	0	$^3A_{2g}$	0 (1.984)	0 (1.903)	0 (1.927)
2	1	3	0	^3E_g (A)	0.12 (1.979)	0.02 (1.900)	0.06 (1.923)
1	1	4	0	$^3B_{2g}$	0.26 (1.983)	0.06 (1.901)	0.08 (1.923)
1	2	3	0	^3E_g (B)	0.74 (1.979)	0.43 (1.895)	0.53 (1.916)
1	2	2	1	$^5A_{1g}$	0.71 (2.063)	1.29 (1.983)	1.12 (2.005)
1	1	3	1	^5E_g	0.85 (2.057)	1.30 (1.975)	1.18 (1.998)
2	1	2	1	$^5B_{2g}$	1.05 (2.061)	1.66 (1.982)	1.49 (2.005)
2	0	4	0	$^1A_{1g}$	1.49 (1.982)	1.46 (1.906)	1.43 (1.927)

[a] Orbital energy levels illustrated in Figure 2. [b] Values in parentheses refer to optimized Fe−N(eq) bond length (in Å) for the pertinent state.

TABLE 2: Calculated Relative Energies (*E*, eV) for Different Configurations in FePn, FeDBPn, and FeHPz

configuration[a]						*E* (R)[b]		
$1a_{1g}/d_{xy}$	$2a_{1g}/d_{z^2}$	$1b_{3g}/d_{yz}$	$1b_{2g}/d_{xz}$	$b_{1g}/d_{x^2-y^2}$	state	FePn	FeDBPn	FeHPz
2	2	1	1	0	$^3B_{1g}(^3A_{2g})$[c]	0 (1.921)	0 (1.887)	0 (1.906, 2.100)[d]
2	1	2	1	0	$^3B_{2g}$ [^3E_g (A)]	−0.13 (1.934)	−0.06 (1.897)	−0.16 (1.906, 2.089)
2	1	1	2	0	$^3B_{3g}$ [^3E_g (A)]	0.18 (1.934)	−0.20 (1.895)	0.37 (1.941, 2.093)
1	1	2	2	0	$^3A_{1g}(^3B_{2g})$	0.47 (1.939)	0.16 (1.907)	0.37 (1.921, 2.087)
1	2	2	1	0	$^3B_{2g}$[^3E_g (B)]	0.64 (1.917)	0.30 (1.892)	0.46 (1.894, 2.069)
1	2	1	1	1	$^5A_{1g}$ ($^5A_{1g}$)	1.32 (1.996)	1.51 (1.956)	0.48 (1.929, 2.215)
1	1	2	1	1	$^5B_{3g}$ (^5E_g)	0.98 (1.996)	1.05 (1.964)	0.36 (1.929, 2.205)
2	1	1	1	1	$^5A_{1g}$ ($^5B_{2g}$)	0.95 (2.014)	0.96 (1.970)	0.77 (1.916, 2.235)
2	0	2	2	0	$^1A_{1g}$ ($^1A_{1g}$)	1.58 (1.940)	1.53 (1.910)	0.57 (1.885, 2.066)

[a] Orbital energy levels illustrated in Figure 2. [b] Values in parentheses refer to optimized Fe−N(eq) bond length (in Å) for the pertinent state. [c] States in parentheses refer to the corresponding designations in FeP (Table 1). [d] The two values in parentheses refer to the Fe−N1 and Fe−N2 bond lengths, respectively (see Figure 1f).

b_{2g} (d_{xy}), and e_g (d_π, i.e., d_{xz} and d_{yz}). For MPn, MDBPn, and MHPz, the symmetry is D_{2h}, as shown by previous calculations on free-base molecules.[33−37] The different occupancies of six electrons in these d orbitals can yield a number of possible low-lying electronic states. The purpose of this paper is to elucidate the ground state and several low-lying excited states that are usually considered in the literature. Geometry optimization was performed for all states of each molecule. Since the structures of the metal macrocycles are highly symmetric and rigid, the geometry optimization can be expected to converge to a minimum. The excellent agreement between the calculated and available experimental bond lengths supports this point of view. The ADF program allows one to assign electrons to specific molecular orbitals (MOs), and therefore, every state can be obtained by explicit occupations of the appropriate MOs. The energetic orderings of the various states are displayed in Tables 1 and 2, along with the optimized Fe−N bond length of each state. Figure 2 illustrates the ground-state MO energy level diagrams of the various unligated Fe^{II} macrocycles (where LUMO = lowest unoccupied MO, HOMO = highest occupied MO).

3.1. Electronic Structure of FeP, FePz, and FePc. As shown in Table 1, the FeP, FePz, and FePc systems all have a $^3A_{2g}$ ground state that arises from the $(d_{xy})^2(d_{z^2})^2(d_\pi)^2$ configuration, in agreement with the experimental assignments of FeTPP (iron tetraphenylporphyrin)[27,28] and FePc.[43] The ^3E_g $[(d_{xy})^2(d_{z^2})^1(d_\pi)^3]$ state is the second lowest. The difference in energy between $^3A_{2g}$ and ^3E_g is 0.12 eV for FeP, in good agreement with Mössbauer measurements of FeTPP that suggest a separation of 0.07 eV.[27] This $^3E_g-{}^3A_{2g}$ energy gap is somewhat smaller in Pc, 0.06 eV. The ^3E_g state of FePz lies only 0.02 eV above $^3A_{2g}$, leaving the identity of the ground state in some doubt. There appears to be some parallel between the $^3E_g-{}^3A_{2g}$ energy gap and the Fe−N bond length in that a longer bond is associated with a larger energy separation.

The lowest quintet state is $^5A_{1g}$. This state lies 0.71 eV above the ground state for FeP, again in good agreement with experiment (0.62 eV) for the similar FeTPP.[28] The energy separation of the $^5A_{1g}$ state from the ground state rises to more than 1 eV for FePz and FePc. There is a good correlation between the Fe−N bond length (i.e., the macrocycle size) and the $^5A_{1g}-{}^3A_{2g}$ energy gap. For a given system, the bond length of the quintets is about 0.08 Å greater than that of the triplets (or of the $^1A_{1g}$ singlet). This longer bond is ascribed to the occupancy of the σ-antibonding b_{1g} ($d_{x^2-y^2}$) orbital in the quintets. In comparison to FeP, the meso tetraaza substitutions significantly reduce the Fe−N bond length in FePz/Pc, while the effects of tetrabenzo annulations lengthen the bond by 0.02 Å: The Fe−N bond lengths vary in the order FeP > FePc > FePz.

With regard to Figure 2, the substitution of nitrogens for the meso CH groups (i.e., P → Pz) lowers the energies of all valence MOs, particularly a_{2u}. The size of the latter shift can be easily understood, since the a_{2u} orbital is mainly concentrated in the meso position.[44] The separation between ring orbitals a_{1u} and a_{2u}, quite small in FeP, is as large as 1 eV in FePz. The smaller core size of Pz splits the metal $b_{1g}/d_{x^2-y^2}$ away from the other d orbitals to a greater extent than does P. The position of b_{1g} is nearly unchanged from FeP to FePz, indicating that the downshifting effect of the aza bridges is canceled by the upshifting effect of the core size.

The transition from Pz to Pc is accompanied by the addition of benzo rings to the cycle. This substitution destabilizes the MOs for the most part, particularly a_{1u}. The a_{1u} orbital contains a large contribution from the β-carbon, and so, the tetrabenzo annulations cause a larger energy shift for a_{1u} than for other orbitals. The separation between a_{1u} and a_{2u} is even larger in FePc than in FePz. The former is destabilized to the point where it lies above the metal b_{2g}/d_{xy} orbital.

3.2. Electronic Structure of FePn, FeDBPn, and FeHPz. Table 2 displays the calculated relative energies for various configurations in FePn, FeDBPn, and FeHPz. The states are listed in the same order as in Table 1, to more clearly emphasize changes in energy ordering caused by the change of the

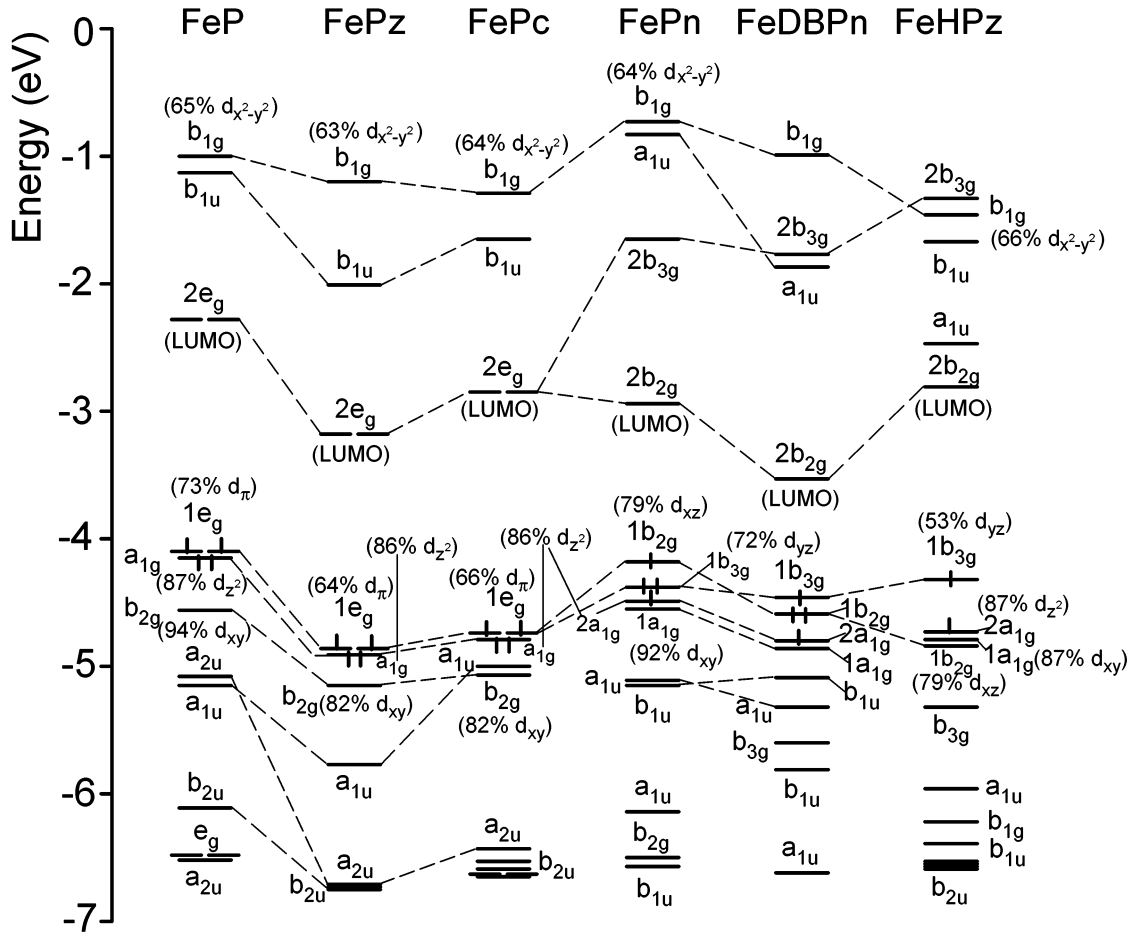

Figure 2. Orbital energy levels of various (unligated) Fe^{II} macrocycles.

macrocycle. With regard to FePn first, the D_{2h} symmetry of Pn removes the $d_{xz}-d_{yz}$ degeneracy, as shown in Figure 2. Therefore, the ^3E_g $[(d_{xy})^2(d_{z^2})^1(d_\pi)^3]$ state in FeP is split into the $^3B_{2g}$ $[(d_{xy})^2(d_{z^2})^1(d_{xz})^2(d_{yz})^1]$ and $^3B_{3g}$ $[(d_{xy})^2(d_{z^2})^1(d_{xz})^1(d_{yz})^2]$ states in FePn. In contrast to FeP's $^3A_{2g}$ $[(d_{xy})^2(d_{z^2})^2(d_\pi)^2]$ ground state, the $^3B_{2g}$ state is the ground state for FePn, and it lies 0.13 eV below the $^3B_{1g}$ (i.e., $^3A_{2g}$ in FeP) state. But the other state $^3B_{3g}$ is destabilized significantly, and it is ~0.2 eV higher than the $^3B_{1g}$ state. The lowest quintet in FePn is now $^5A_{1g}$ ($^5B_{2g}$), which lies 0.95 eV higher in energy than $^3B_{1g}$, or 1.08 eV higher than the ground state. According to the calculations, the Fe−N bond length in FePn is about 0.06 Å smaller than that in FeP. The smaller core size of Pn increases the splitting of the $d_{x^2-y^2}$ level from the other d orbitals (as shown in Figure 2), which makes the high-spin state less accessible than in P complexes. The symmetry lowering from P to Pn also reverses the energy order of the quintets. As also shown in Figure 2, the $2e_g$ (π^*) MOs, degenerate in P, are split considerably as a result of the reduced symmetry of the macrocycle. Therefore, the energy gap between the LUMO and the HOMO in FePn is notably smaller than in FeP. This trend is in agreement with electrochemical determinations.[21]

In comparison to the structure of Pn, DBPn has two fused six-membered rings through the pyrrole β-carbons. An extended conjugation of the macrocycle stabilizes most MOs, particularly the empty $2b_{2g}$ and a_{1u} orbitals. But the $1b_{3g}/d_{yz}$ orbital, which is the HOMO−1 in FePn, is not stabilized notably and becomes the HOMO in FeDBPn. Therefore, the LUMO−HOMO gap of FeDBPn is even smaller than that of FePn. The dibenzo rings also result in a further splitting of the $2e_g$ (π^*) orbitals. Different somewhat from FePn, FeDBPn has a ground state of $^3B_{3g}$, followed by $^3B_{2g}$ and $^3B_{1g}$. The Fe−N bond in FeDBPn is about 0.04 Å contracted as compared to that in FePn.

FeHPz has a ground state of $^3B_{2g}$, similar to FePn. The $^3B_{1g}$ ($^3A_{2g}$) state is the second lowest, 0.16 eV higher than the ground state. $^5B_{3g}$ (^5E_g) is now calculated to be the lowest quintet; it is only 0.52 eV above the ground state and essentially degenerate with the $^3B_{3g}$ and $^3A_{1g}$ states. The calculations show strong inequivalence of the pairs of the inner nitrogens, with R_{Fe-N1} being 0.18 Å shorter than R_{Fe-N2} in the ground state. As a result, there is a much larger $d_{xz}-d_{yz}$ splitting in FeHPz than in FePn or in FeDBPn. The $1b_{3g}$ orbital represents the HOMO of FeHPz, similar to FeDBPn. But the d_{yz} character (53%) of the HOMO in FeHPz is considerably reduced.

3.3. Structural and Energetic Properties. The calculated properties of the various Fe^{II} macrocycles in the ground state are collected in Table 3, together with available experimental Fe−N bond lengths for comparison. The Fe-macrocycle binding energy E_{bind} is defined as the energy required to pull the metal away from the ring. In the case of FeP, for example, we have

$$-E_{bind} = E(\text{FeP}) - \{E(\text{Fe}) + E(\text{P})\}$$

where E(FeP), E(Fe), and E(P) represent the total energies of FeP, Fe, and P, respectively. (The geometry of P is independently optimized.)

The ionization potentials (IPs) and electron affinities (EAs) were calculated by the so-called ΔSCF method which carries out separate SCF (self-consistent field) calculations for the molecule and its ion, where IP = $E(X^+) - E(X)$ and EA = $E(X^-) - E(X)$.

TABLE 3: Calculated Fe−N Bond Lengths (R_{Fe-N}, Å), Fe-macrocycle Binding Energies (E_{Bind}, eV), Charge Distribution on Fe (Q_{Fe}, e), Ionization Potentials (IP, eV) and Electron Affinities (EA, eV) at the Ground State of the (unligated) Iron Complexes

		FeP	FePz	FePc		FePn	FeDBPn	FeHPz
R_{Fe-N}	calcd	1.984	1.903	1.927		1.934	1.895	1.906, 2.089[a]
	exptl	1.972[b]		1.927[c]		1.932[d]		
	ΔR[e]	0.081	0.007	0.022		−0.052	0.025	0.014, 0.114
	E_{bind}	10.25	11.51	9.81		10.61	8.78	9.33
	Q_{Fe}	0.66	0.77	0.72		0.75	0.74	0.71
IP	a_{1g}/d_{z^2}	6.29 (first)	6.87 (first)	6.51	$1b_{3g}/d_{yz}$	6.39 (first)	6.82	6.51 (first)
	b_{2g}/d_{xy}	6.63	7.01	6.67	$1a_{1g}/d_{xy}$	6.82	6.73	6.56
	a_{2u}	7.00	8.71	7.85	a_{1u}	7.01	7.16	7.49
	a_{1u}	7.01	7.65	6.46 (first)	b_{1u}	7.04	6.93	6.77 (b_{3g})
	$1e_g/d_\pi$	7.26	7.79	7.34	$1b_{2g}/d_{xz}$	7.30	6.30 (first)	6.55
EA	$1e_g$	−1.66	−2.54	−2.55		−1.89 ($1b_{2g}$)	−2.58 ($2b_{2g}$)	−2.27 ($2a_{1g}$)
	$2e_g$	−1.32	−2.18	−2.10		−1.88 ($2b_{2g}$)	−2.50 ($2a_{1g}$)	−2.11 ($1b_{3g}$)
						−1.42 ($2a_{1g}$)	−2.46 ($1b_{3g}$)	−1.98 ($2b_{2g}$)

[a] The two values refer to the Fe−N1 and Fe−N2 bond lengths, respectively (see Figure 1f). [b] X-ray diffraction data on FeTPP (ref 45). [c] ref 46. [d] X-ray diffraction data on FeTPrPn (ref 25c). [e] ΔR represents the contraction of the ring core size when the macrocycle is complexed with Fe; for FeP, for example, $\Delta R = R_{center\cdots N}$ (P, without H atoms in the cage) − R_{Fe-N} (FeP).

The calculated Fe−N bond lengths (R_{Fe-N}) are 1.98 Å for FeP and 1.93 Å for FePc, in very good agreement with the experimental values for solid FeTPP (1.97 Å)[45] and FePc (1.93 Å).[46] Replacement of P by Pz shortens R_{Fe-N} by 0.08 Å; this bond is, however, lengthened by 0.02 Å when going from Pz to Pc. The change in symmetry from P (D_{4h}) to Pn (D_{2h}) shortens the Fe−N bond by 0.05 Å. There are X-ray crystal structure data available for FeTPrPn wherein R_{Fe-N} is 1.932 Å,[25c] which compares excellently with the calculated value (1.934 Å) for FePn. Extending the π-conjugation of the molecule (i.e., Pn → DBPn) results in a further shortening of this bond by 0.04 Å. In FeHPz, the Fe−N1 and Fe−N2 bonds are strongly inequivalent, with R_{Fe-N2} being 0.18 Å longer than R_{Fe-N1}.

To obtain some idea about the rigidity of the macrocycle frame, Table 3 also lists ΔR values, which represent a contraction or expansion of the ring core size when the macrocycle is complexed with Fe. Most macrocycles are more or less contracted upon complexation with the metal. Pn is the only exception, where the core size is expanded by ∼0.05 Å. Free-base DBPn has a larger core size than the corresponding Pn, but the opposite is the case for the metal complexes.

The energetic measures of the interactions of the metal with the rings are generally consistent with the trend in the Fe−N bond length. The binding energy goes up by 1.3 eV upon the change of the ring from P to Pz, as R_{Fe-N} becomes considerably shorter. The trend is in agreement with the electrochemical result which indicates that the Pz ring stabilizes M^{II} relative to a P ring. The opposite occurs when the four benzo rings of Pc are added to Pz, making the Fe−Pc binding energy even smaller than the Fe−P one. A similar situation is found for the binding energy change from FeP to FePn to FeDBPn.

The "effective" charge of Fe (Q_{Fe}) lies in the range 0.65−0.75 e and does not change much from one macrocycle to another. In general, a smaller ring core size causes a little more effective charge transfer from the metal to the ring. The oxidation state of Fe in the various macrocycles here is formally described as Fe^{II}. The calculated rather small Q_{Fe} indicates that the bond between Fe and N in not purely ionic but significantly covalent.

The ionization potentials (IPs) of FePz are raised significantly when the meso CH groups are changed to the N atoms of Pz. This is reflected in electrochemical data:[47] The oxidation potentials of Fe^{II} porphyrazines are positively shifted by as much as 400 mV as compared to analogous porphyrins. For both FeP and FePz, the first ionization occurs from the metal a_{1g}/d_{z^2} orbital. In the case of FePc, however, the first ionization now takes place from the ring a_{1u} orbital, and the calculated first IP is significantly smaller than that of FePz. This orbital is a candidate for ionization, as it lies near the HOMO level in the neutral FePc system, and the decrease of the IP is a consequence of the destabilization of the a_{1u} orbital in Pc, induced by the benzo ring. Concerning the electron affinities, there is a considerable increase in the EA from FeP to FePz, whereas little additional change occurs upon adding the benzo rings of FePc. The added electron goes into the low-lying half-filled $1e_g/d_\pi$ orbital for each of the three systems.

In contrast to FeP, the first ionization for FePn now occurs from the $1b_{3g}/d_{yz}$ orbital, yielding a $(2a_{1g})^1(1b_{3g})^1(1b_{2g})^1$ ground state for $[FePn]^+$. But the calculated first IP of FePn is similar to that of FeP. From FePn to FeDBPn, the ordering of the $1b_{2g}$ and $1b_{3g}$ orbitals is changed, and so, the first ionization for FeDBPn takes place from the $1b_{2g}/d_{xz}$ orbital; the dibenzo rings of DBPn have no obvious effect on the first IP. In the case of FeHPz, the first ionization occurs from the singly occupied HOMO $1b_{3g}/d_{yz}$, owing to a large energy gap between the $1b_{3g}$ and $1b_{2g}$ orbitals. The calculated first IP of FeHPz is about 0.2 eV larger than that of FeDBPn.

Although there is no notable downshift of the HOMO level from FeP to FePn, the latter system has a larger EA than the former one by 0.23 eV. This difference in EA between FePn and FeP can be attributed to the difference in the electronic structure. For FeP, the added electron goes to the $1e_g$ orbital first, yielding a $(d_{z^2})^2(d_\pi)^3$ state, which is, however, not the ground state for $[FeP]^-$. In the case of FePn, the added electron enters the $1b_{2g}$ orbital to yield a $(d_{z^2})^1(d_\pi)^4$ state (ground state), which is about 0.25 eV lower in energy than the $(d_{z^2})^2(d_\pi)^3$ state for a given system. On the other hand, the addition of an electron to the high-lying Pn $2b_{2g}$ orbital (LUMO) yields only a 0.01-eV smaller EA than that to the $1b_{2g}$ orbital. This feature results from lowering the LUMO energy of the Pn system as compared to P; i.e., the quite low LUMO in FePn makes this orbital relatively easily accessible for an incoming electron. If the metal (M) is Ni, Cu, or Zn, where the 3d orbitals are low in energy, the first electron is added to the porphyrin $2e_g$ (π^*) orbital. In this case, the calculated EA for the porphycene can be 0.5−0.6 eV larger than that for the analogous porphyrin. This result is in agreement with the experimental observation[9,15,26] that the Pn macrocycle is easier to reduce than the P one. Both macrocycles exhibit another noticeable difference in their reduction:[14] Only two distinct reductions steps are observed in the porphycenes, instead of four steps in the porphyrins. This can also be understood from the difference in the electronic

TABLE 4: Calculated Properties[a] of the Ligated Iron Complexes

	$R_{Fe-N(eq)}$ (Å)	$R_{Fe-L(ax)}$ (Å)	E_{bind} (eV)[FeP−$(L)_2$]	Q_{Fe}	IP[e] (eV)	EA[e] (eV)
$FeP(Py)_2$	1.998	2.023	1.44	0.73	5.91 (a_{1g}), 5.67 ($1b_{2g}$), 5.70 ($1b_{3g}$), 6.33 (b_{1u})	−0.99 ($2b_{2g}$)
FeP(Py)(CO)	2.006	2.104[b]	2.00	0.52	6.53 ($2a_1$), 6.67 ($1b_1$), 6.68 ($1b_2$), 6.71 ($1a_1$)	−1.17 ($2b_1$)
		1.747[c]				
		0.017[d]				
FeP(CO)	1.997	1.697	1.41	0.58	7.12 (b_2), 7.15 (1e), 7.05 (a_2)	−1.37 (2e)
		0.167[d]				
$FePz(Py)_2$	1.923	2.040	1.59	0.79	6.35 (a_{1g}), 6.22 ($1b_{2g}$), 6.26 ($1b_{3g}$), 6.98 (a_{1u})	−1.66 ($2b_{2g}$)
FePz(Py)(CO)	1.934	2.117	1.96	0.57	7.00 ($2a_1$), 7.13 ($1b_1$), 7.14 ($1b_2$), 7.35 (a_2)	−1.96 ($2b_2$)
		1.760				
		0.030				
FePz(CO)	1.921	1.702	1.37	0.66	7.50 (b_2), 7.71 (1e), 7.70 (a_2)	−2.22 (2e)
		0.186				
$FePc(Py)_2$	1.945	2.031	1.69	0.75	6.19 (a_{1g}), 6.06 ($1b_{2g}$), 6.08 (a_{1u}), 6.11 ($1b_{3g}$)	−1.71 ($2b_{3g}$)
FePc(Py)(CO)	1.955	2.122	2.08	0.53	6.29 (a_2), 6.79 (a_1), 6.87 ($1b_1$), 6.88 ($1b_2$)	−1.95 ($2b_2$)
		1.753				
		0.021				
FePc(CO)	1.942	1.702	1.39	0.63	6.51 (a_2), 7.17 (b_2), 7.29 (1e)	−2.15 (2e)
		0.165				
$FePn(Py)_2$	1.951	2.004	1.27	0.78	5.37 ($1b_{2g}$), 5.82 (a_{1g}), 5.64 ($1b_{3g}$), 6.46 (a_{1u})	−1.61 ($2b_{2g}$)
FePn(Py)(CO)	1.963	2.073	1.86	0.54	6.60 ($2a_1$), 6.45 ($1b_1$), 6.66 ($1b_2$), 6.78 (a_2)	−1.80 ($2b_1$)
		1.745				
		0.033				
FePn(CO)	1.948	1.684	1.14	0.63	6.98 ($2a_1$), 6.98 ($1b_1$), 7.17 ($1b_2$), 7.09 (a_2)	−1.98 ($2b_1$)
		0.160				
$FeDBPn(Py)_2$	1.917	2.016	1.43	0.81	5.68 ($1b_{3g}$), 6.00 (a_{1g}), 5.73 ($1b_{2g}$), 6.26 (b_{1u})	−2.13 ($2b_{2g}$)
FeDBPn(Py)(CO)	1.929	2.089	1.79	0.54	6.40 ($2a_1$), 6.32 ($1b_2$), 6.60 ($1b_1$), 6.52 (a_1)	−2.35 ($2b_1$)
		1.754				
		0.029				
FeDBPn(CO)	1.917	1.698	1.18	0.60	6.86 ($2a_1$), 6.68 (b_2), 7.02 ($1b_1$), 7.00 ($1a_1$)	−2.57 ($2b_1$)
		0.206				
$FeHPz(Py)_2$	1.950	2.012	1.28	0.70	5.48 ($1b_{3g}$), 6.09 (a_{1g}), 6.22 ($1b_{2g}$), 6.36 (b_{3g})	−1.64 ($2b_{2g}$)
	2.111					
FeHPz(Py)(CO)	1.955	2.095	1.75	0.49	6.11 ($1b_2$), 6.78 (a_1)	−1.88 ($2b_1$)
	2.132					
		1.746				
		0.019				
FeHPz(CO)	1.943	1.694	1.07	0.61	6.46 ($1b_2$), 7.20 (a_1), 7.43 (b_2), 7.79 ($1b_1$)	−2.09 ($2b_1$)
	2.111					
		0.162				

[a] $R_{Fe-N(eq)}$: equatorial Fe−N bond length. $R_{Fe-L(ax)}$: axial Fe-L bond length. IP: ionization potential. EA: electron affinity. [b] Fe−N(ax) bond length. [c] Fe−C(ax) bond length. [d] Fe out-of-plane displacement toward CO. [e] See Figures 3−5 for the orbitals in parentheses; the first IP is indicated in bold.

structure between MP and MPn. In MP, the $2e_g$ orbitals are the LUMO and are able to accept four electrons, while in MPn, the LUMO is $2b_{2g}$ and can only accept two electrons. The LUMO+1 ($2b_{3g}$) level in MPn is too high to be accessible to incoming electrons. Since the P → Pn replacement does not change the IP very much, this also accounts for the experiment finding[15] that the oxidation characteristics of a porphycene parallel those of a porphyrin.

The dibenzo rings of DBPn have a large effect on electron affinity. As is evident from Table 3, the EA is increased by ∼0.7 eV from FePn to FeDBPn. Thus, the reduction is even more facile in DBPn compounds than in Pn compounds. For FeHPz, an added electron is accommodated in the lower-lying $2a_{1g}/d_{z^2}$ orbital, which is different from the situation of FePn or FeDBPn. This difference may be ascribed to a relatively large energy gap between the HOMO ($1b_{3g}$) and HOMO−1 ($2a_{1g}$) in FeHPz. The calculated EA of FeHPz is intermediate between those of FePn and FeDBPn.

3.4. Axial Ligation of Pyridine (Py) and CO. This section is concerned with an elucidation of the properties of the various ligated Fe^{II} macrocycles. The axial ligands considered here include CO as a strong π-acceptor and pyridine (Py) which has a strong σ-donor capacity but is a relatively weak π-bonder. In a solution of pure Py, the Fe^{II} macrocycle is able to add two Py molecules to form a six-coordinate species [-$(Py)_2$].[25] If there are CO molecules present in the solution, one Py ligand can be replaced by CO, giving rise to a −(Py)(CO) species. Recently, five-coordinate ruthenium porphyrins associated with one CO molecule, RuP(CO), were observed in the gas phase by Shafizadeh et al.,[48,49] and so, the MP(CO) molecules are interesting. Here, all three types of the ligated Fe^{II} macrocycles were investigated. The calculated properties are collected in Table 4. The structures of the complexes were optimized under D_{2h} [for -$(Py)_2$ species] and C_{2v} [for -(Py)(CO) and -(CO) species] symmetries, respectively, where the Py ring plane is perpendicular to the macrocycle and bisects its N−Fe−N angles; the Fe−CO attachment is linear, as evidenced by other theoretical calculations on related systems.[50a−c] Effects of axial ligands upon the valence MO levels of FeP are displayed in Figure 3; the left and right extremes of Figure 3 represent the energy levels of the unperturbed Py and CO ligands. Figures 4 and 5 illustrate valence orbital energy levels for the other ligated Fe^{II} macrocycles.

3.4.1. FeP(Py)$_2$, FeP(Py)(CO), and FeP(CO). As illustrated in Figure 3, the repulsive interaction between the ligand HOMO and the Fe a_{1g}/d_{z^2} orbital dramatically raises the energy of the latter. This rise of the a_{1g} orbital results in a low-spin, closed-shell [$(d_{xy})^2(d_{xz})^2(d_{yz})^2$] complex. The d_{xz} and d_{yz} degeneracy is removed, since the symmetry is lowered from D_{4h} to D_{2h}. As mentioned above, Py is an electron-donating ligand, which shifts

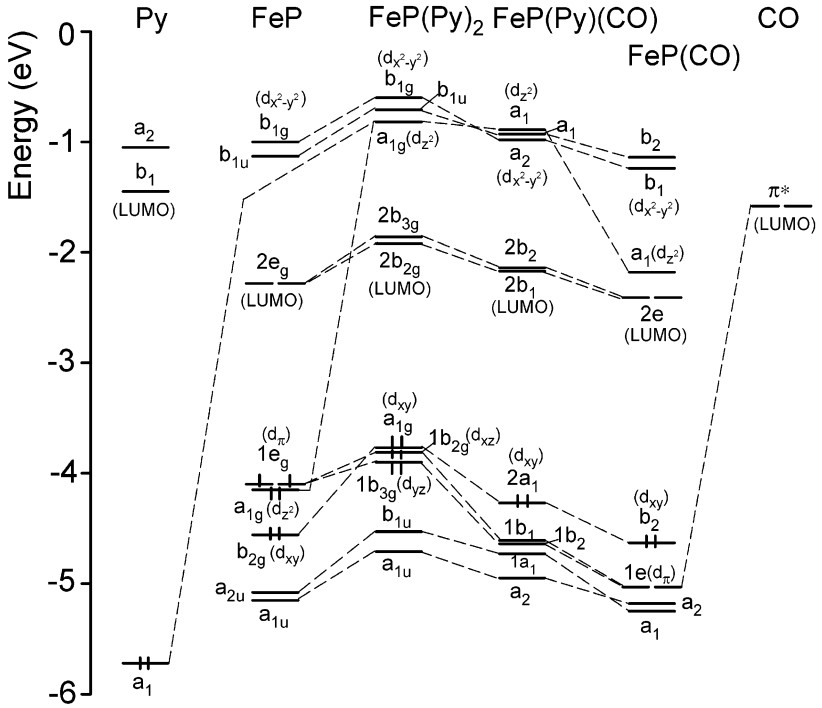

Figure 3. Orbital energy levels of FeP complexed with axial ligands, as well as unligated FeP and ligands (Py, CO) for purpose of comparison.

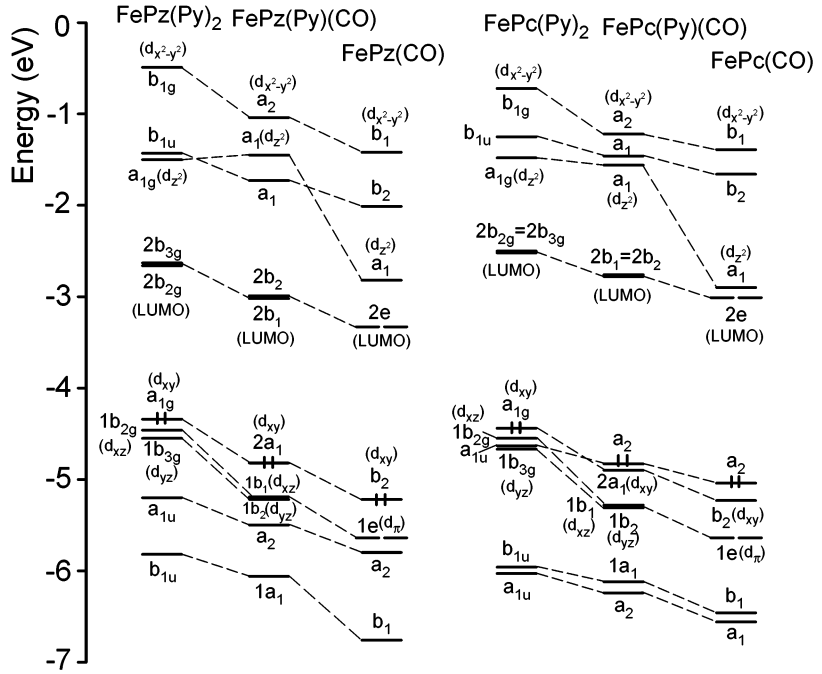

Figure 4. Orbital energy levels of FePz and FePc complexed with axial ligands.

the valence MOs of FeP upward. The b_{2g}/d_{xy} orbital of FeP is shifted enough so that it (transferred to a_{1g} in ligated FeP) becomes the HOMO of the system. The first ionization in FeP-$(Py)_2$ arises from the metal $1b_{2g}/d_{xz}$ orbital (HOMO−1); ionization from the HOMO a_{1g}/d_{xy} requires 0.24 eV more energy, and from b_{1u} (P−a_{2u}) a further 0.4 eV. Compared to FeP, the first IP of $FeP(Py)_2$ is decreased by 0.6 eV, suggesting that the axial ligands of $FeP(Py)_2$ ease the oxidation. The ligands also decrease the electron affinity of the assembly from −1.7 to −1.0 eV. Note that the added electron in $FeP(Py)_2$ occupies a high-lying, antibonding P−$2b_{2g}$ orbital, whereas the added electron in FeP goes into a low-lying metal orbital. The E_{bind} entry in Table 4, which refers to the binding energy between the Fe^{II} macrocycle and the axial ligand(s), indicates that the two Py ligands are bound to the complex by about 1.4 eV. Addition of the two Py ligands expands the equatorial Fe−N distance ($R_{Fe-N(eq)}$) by a small amount (less than 0.02 Å). These ligands also slightly increase the positive charge of the metal atom.

Replacement of one of the Py ligands by CO lowers all of the MOs. The d_{xz} and d_{yz} orbitals are particularly stabilized, which may be attributed to Fe → CO π^* back-bonding, as illustrated in Figure 3. The first ionization of FeP(Py)(CO), unlike $FeP(Py)_2$, occurs from the HOMO $2a_1/d_{xy}$, but requires 0.9 eV more energy than the first IP in $FeP(Py)_2$. The latter result is consistent with the experimental observation that the

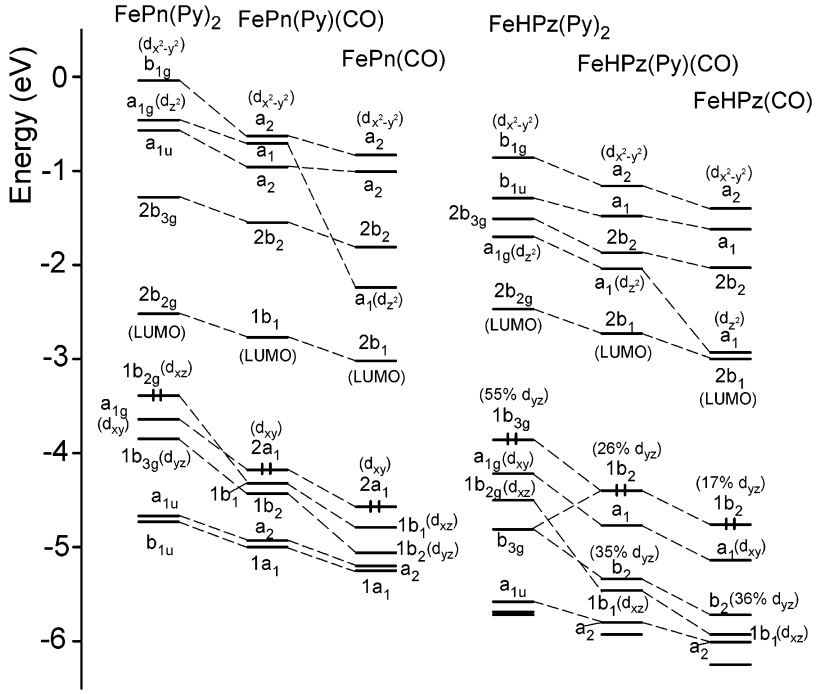

Figure 5. Orbital energy levels of FePn and FeHPz complexed with axial ligands.

TABLE 5: Comparison of the Present Calculated Results of FeP(Py)(CO) and FeP(CO) with Those Obtained by Other Calculations

system	method	$R_{Fe-N(eq)}$ (Å)	$R_{Fe-N(ax)}$ (Å)	$R_{Fe-C(ax)}$ (Å)	R_{C-O} (Å)	E_{bind} (eV) (FeP−CO)
FeP(Py)(CO)	VWN−B−P[a]	2.01	2.10	1.75	1.16	1.39
FeP(Im)(CO)	CPMD[b]	2.02	2.07	1.72	1.17	1.52
	PEB[c]	1.99	1.96	1.79	1.16	
	LDF[d]	1.98	1.97	1.73	1.16	
	Exptl[e]	2.02(1)	2.10(1)	1.77(2)	1.12(2)	
FeP(CO)	VWN−B−P[a]	2.00		1.70	1.16	1.41
	CPMD[b]	1.99		1.69	1.17	1.13

[a] Present ADF calculations using VWN−B−P functional. [b] DFT calculations by Rovira et al. based on Carr-Parinello molecular dynamics method (ref 50a). [c] DFT calculations by Han et al. using Perdew-Burke-Ernzerhof functional (ref 50b). [d] Local density functional calculations by Ghosh and Bocian (ref 50c). [e] Experimental distances in crystal FeTPP(Py)(CO) (ref 52).

oxidation potential is increased on going from $MP(Py)_2$ to MP(Py)(CO).[51] The IP of the lower $1a_1$ orbital, derived from $P-a_{2u}$, is increased by only 0.38 eV [relative to that of $FeP(Py)_2$]. Therefore, the IPs of $Fe-d_{xy}$ and $P-a_{2u}$ for FeP(Py)(CO) are in fact rather close, within 0.2 eV of one another.

There are X-ray diffraction data available for crystalline FeTPP(Py)(CO),[52] which are shown to be in excellent agreement with the calculated bond lengths (see Table 5). Fe lies slightly out of the porphyrin plane (0.02 Å) toward the CO group. The Py/CO tandem is more strongly bound to the complex by 0.56 eV than are a pair of Py ligands, but the CO attachment reduces the Fe−Py binding: $R_{Fe-N(ax)}$ in FeP(Py)(CO) is considerably longer (0.08 Å) than that in $FeP(Py)_2$. On the other hand, The C−O bond length (1.16 Å) increases by 0.02 Å relative to free molecule (1.14 Å), suggesting that the π-back-donation from the metal to CO plays a role in the FeP−CO interaction.

As a model of carbon monohemes, the binding of CO to a FeP(Im) complex (Im = imidazole) was studied by several research groups.[50a−c] Table 5 presents a comparison of the present calculated results of FeP(Py)(CO) with those obtained by other calculations. Though the systems are somewhat different, the various bond lengths as well as the FeP−CO binding energies obtained with the different computational methods are quite close.

The MO levels are further lowered upon removing the Py ligand in FeP(Py)(CO), and the Fe−CO bond is then shortened (by 0.05 Å) and strengthened. Owing to a large attraction by CO, the Fe atom moves 0.17 Å out of the porphyrin plane. The FeP(CO) species was once studied by Parrinello et al.[50a] using a DFT method. As shown in Table 5, the results obtained by those authors also compare favorably with our calculated values. Although the a_1/d_{z^2} orbital is lowered considerably in FeP(CO), it nevertheless remains unoccupied. The first ionization for FeP(CO) now occurs from the porphyrin a_2 ($P-a_{1u}$) orbital. Note that the ordering of the $P-a_{2u}$ and $P-a_{1u}$ orbitals is reversed in FeP(CO). Corresponding to a downshift of the MOs, both the IP and EA of FeP(CO) are larger than those of FeP(Py)(CO).

3.4.2. FePz/Pc(Py)$_2$, FePz/Pc(Py)(CO), and FePz/Pc(CO). The MO energy level diagrams of these complexes are illustrated in Figure 4. Similar to FePz(Py)(CO), the first ionization in FePz(CO) also occurs from the central metal ($Fe-d_{xy}$), in contrast to the case of porphyrin. Unlike FePc, where the first ionization occurs from a Pc orbital, that of $FePc(Py)_2$ takes place from a metal orbital ($1b_{2g}/d_{xz}$). This result is in agreement with experimental observation on $FePc(Py)_2$.[53] We note that for FePc(Py)$_2$ the IP from the $Pc-a_{1u}$ orbital is nearly identical to the first IP, the difference being only 0.02 eV. In the presence of CO, the first ionizations of the ligated FePc species clearly arise from the a_2 ($Pc-a_{1u}$) orbital. This orbital also becomes the HOMO in both FePc(Py)(CO) and FeP(CO), since the metal d orbitals are particularly stabilized owing to Fe → CO π^* back-bonding. The axial ligand binding properties (the Fe−L bond lengths and binding energy) of FePz/Pc are comparable to those of FeP.

3.4.3. The Other Ligated Fe^{II} Macrocycles. The change in symmetry from P to Pn slightly decreases the binding energy between Fe and the axial ligand(s), but no apparent differences in the axial ligand binding properties are found between FePn and FeDBPn. FeHPz exhibits notably smaller affinity toward CO than does FeP (by 0.34 eV). It is reported that FeHPz fails

to coordinate CO in the same conditions as the porphyrin complex does. Although the calculated E_{bind} values are consistent with the experimental trend of the complex stabilities, they may not fully account for why FeHPz is not able to coordinate CO, since the absolute FeHPz−CO binding energy is still as large as 1.1 eV.

Figure 5 displays the MO energy level diagrams of the ligated FePn and FeHPz complexes. A major difference between the ligated FeP and FePn species is that the CO ligand in FePn(CO) cannot change the site of the first ionization from a metal orbital to a macrocycle orbital. The coordination of CO to FeHPz strongly affects the nature of the HOMO. Figure 2 has shown that in FeHPz the HPz−b_{3g} orbital is mixed significantly with the dominant Fe−d_{yz} in the HOMO. In FeHPz(Py)(CO), however, the Fe−d_{yz} orbital makes a contribution of only 26% to the HOMO, and in FeHPz(CO), the character of Fe−d_{yz} is further decreased. The first ionizations in the ligated FeHPz species all arise from the HOMO, the nature of which is changed from a predominantly metal orbital in FeHPz(Py)$_2$ to a predominantly macrocycle orbital in FeHPz(CO).

3.5. Electronic Structure of the Ions: Oxidation and Reduction Properties. One of the striking features of the metal macrocycles is their ability to undergo facile oxidation and reduction. Successive formation of the $[MP/Pc]^{x+}$ ($x = 1, 2$) and $[MP/Pc]^{y-}$ ($y = 1, 2, 3, 4$) ions has been observed for a number of metal complexes.[54,55] However, the character of the acceptor orbitals is not well-understood for some of the reduced species, nor is the nature of the oxidized species, i.e., whether the metal or macrocycle is oxidized. In this section, we provide a description of the electronic structure of the mono- and dipositive and -negative ions for the various unligated and ligated Fe macrocycles. The calculated relative energies for selected configurations are collected in Table 6. The oxidation state of Fe in each ion is reported in the last column of the table, together with the calculated first and second ionization potentials, whose values should aid in future work on photoelectron spectra of these molecules. The first oxidation and reduction of each system have been discussed in sections 3.3 and 3.4. We now turn our attention mainly to the second redox processes.

The ground state of $[FeP]^{2+}$ corresponds to the $(a_{2u})^1(d_{xy})^2(d_{z^2})^1(d_\pi)^2$ configuration; thus, the second oxidation of FeP now takes place from the macrocycle. For FePz, the second oxidation occurs also from the macrocycle, namely from Pz−a_{1u}, but electron extraction from the metal b_{2g}/d_{xy} orbital requires only 0.1 eV more energy. FePc is different, favoring a second oxidation from the metal. The first and second reductions of FeP/Pz/Pc to yield $[FeP/Pz/Pc]^-$ and $[FeP/Pz/Pc]^{2-}$ involve electron addition to the low-lying half-filled metal d orbitals.

Similar to FeP, the second oxidations in both FePn and FeDBPn occur from the macrocycle. FeHPz is different, since both its first and second oxidations occur from the central metal. Owing to a low-lying LUMO in the D_{2h} species, the second reduction in both the FePn and FeHPz species involves electron addition to the macrocycle, but it involves electron addition to the metal in FeDBPn. Note that the first reduction orbitals in FePn and FeHPz are different from that in FeDBPn.

With coordination of two Py axial ligands to FeP, the second oxidation in FeP(Py)$_2$ occurs from the metal, in contrast to the case in unligated FeP. The same is true in FeP(Py)(CO) and FeP(CO). When the macrocycle is Pz, there is a change of the oxidation site from $[FePz(Py)_2]^{2+}$ to $[FePz(Py)(CO)]^{2+}$. While the first oxidation in FePc(Py)$_2$ occurs from the macrocycle, the second oxidation of the species now arises from the metal. But when one of the Py ligands is replaced by CO, the second oxidation again occurs from the macrocycle.

FePn(Py)$_2$ and FePn(Py)(CO) show similar behavior to the corresponding FeP species upon oxidation, but FePn(CO) is different from FeP(CO) in the case of the first oxidation. No difference in the oxidation site is found between the ligated FePn and FeDBPn species. All ligated FeHPz species undergo their first and second oxidations from the HOMO, but the character of the HOMO is different for different species, as is shown in Figure 5. For FeHPz(Py)$_2$, the HOMO is principally Fe−d_{yz}, while it is predominantly a macrocycle orbital for the carbonyl complexes of FeHPz.

Concerning reductions in the ligated species, all of which have a closed-shell ground state, the first two electrons are added to the LUMO, which is a high-lying antibonding macrocycle orbital.

4. Conclusions

The main conclusions are as follows.

(1) The ground states of FeP and FePc are $^3A_{2g}$ $[(d_{xy})^2(d_{z^2})^2(d_\pi)^2]$ with ^3E_g $[(d_{xy})^2(d_{z^2})^1(d_\pi)^3]$ a little (∼0.1 eV) higher in energy, while the $^3A_{2g}$ and ^3E_g states are nearly degenerate for FePz. With decrease in symmetry of the macrocycle from D_{4h} to D_{2h}, the degeneracy of the d_π (d_{xz}, d_{yz}) orbitals is lifted, and $^3B_{2g}$ $[(d_{xy})^2(d_{z^2})^1(d_{yz})^2(d_{xz})^1]$ or $^3B_{3g}$ $[\cdots(d_{yz})^1(d_{xz})^2]$ becomes the ground state for FePn, FeDBPn, and FeHPz.

(2) The first oxidation for FePc occurs at the macrocycle, in contrast to the metal oxidation for the other Fe^{II} macrocycles.

(3) The ionization potentials (IPs) are increased from FeP to FePz but decreased greatly from FePz to FePc. The first IPs vary in the order FeP (6.29 eV) ≈ FeDBPn (6.30 eV) < FePn (6.39 eV) < FePc (6.46 eV) < FeHPz (6.51 eV) < FePz (6.87 eV).

(4) While the first reduction for every Fe^{II} macrocycle involves electron addition to a metal d orbital, the calculated electron affinities (EAs) are different for different systems and vary in the order FeP (−1.66 eV) < FePn (−1.89 eV) < FeHPz (−2.27 eV) < FePz (−2.54 eV) ≈ FePc (−2.55 eV) ≈ FeDBPn (−2.58 eV). The calculated IP and EA values as well as the orbital energy level diagrams may account for the experimental observation[15] that metal porphycenes (MPn) and metal porphyrins (MP) exhibit quite similar electrochemical behavior upon electrooxidation but not upon electroreduction.

(5) The smaller core size of the macrocycle results in a stronger ligand field in Pz/Pn than in P. However, the benzo annulation (in Pc/DBPn) produces a large destabilizing effect on the metal−macrocycle bonding.

(6) There are also significant changes in the calculated properties of the ligated metal complexes upon variation of the macrocycle framework. Our clear elucidation of the electronic structures of the mono- and dipositive and -negative ions for various unligated and ligated iron macrocycles allows understanding of the observed electronic properties and also would be quite useful for future electrochemical or related work on these compounds.

Appendix. Ionization Properties of RuP(CO)

Recently, Shafizadeh et al.[49] reported the observation of a gas-phase, doubly charged $[RuOEP(CO)]^{2+}$ ion through multiphoton excitation, but the localization of the charges (i.e., whether they are localized on the metal or on the macrocycle) is unclear. Sections 3.4.1 and 3.5 have shown that the first and second ionizations of FeP(CO) occur from the macrocycle and the central metal, respectively. Ru compounds often show

TABLE 6: Calculated Relative Energies (*E*, eV) for Selected Configurations in Various Positive and Negative Ions[a]

system	configuration (see Figures 2−5)	*E*	oxidation state on Fe
$[FeP]^{1+}$	$(a_{2u})^2(b_{2g}/d_{xy})^2(a_{1g}/d_{z^2})^1(1e_g/d_\pi)^2$	0	Fe^{III} (IP_1: 6.29)
	$(a_{2u})^2(b_{2g}/d_{xy})^1(a_{1g}/d_{z^2})^2(1e_g/d_\pi)^2$	0.34	
	$(a_{2u})^1(b_{2g}/d_{xy})^2(a_{1g}/d_{z^2})^2(1e_g/d_\pi)^2$	0.71	
$[FeP]^{2+}$	$(a_{2u})^1(b_{2g}/d_{xy})^2(a_{1g}/d_{z^2})^1(1e_g/d_\pi)^2$	0	Fe^{III} (IP_2: 10.55)
	$(a_{2u})^2(b_{2g}/d_{xy})^1(a_{1g}/d_{z^2})^1(1e_g/d_\pi)^2$	0.69	
$[FeP]^{1-}$	$(b_{2g}/d_{xy})^2(a_{1g}/d_{z^2})^2(1e_g/d_\pi)^3$	0	Fe^{I}
	$(b_{2g}/d_{xy})^2(a_{1g}/d_{z^2})^2(1e_g/d_\pi)^2(2e_g)^1$	0.34	
$[FeP]^{2-}$	$(b_{2g}/d_{xy})^2(a_{1g}/d_{z^2})^2(1e_g/d_\pi)^4$	0	Fe^{0}
	$(b_{2g}/d_{xy})^2(a_{1g}/d_{z^2})^2(1e_g/d_\pi)^3(2e_g)^1$	0.45	
$[FePz]^{1+}$	$(a_{1u})^2(b_{2g}/d_{xy})^2(a_{1g}/d_{z^2})^1(1e_g/d_\pi)^2$	0	Fe^{III} (IP_1: 6.87)
	$(a_{1u})^2(b_{2g}/d_{xy})^1(a_{1g}/d_{z^2})^2(1e_g/d_\pi)^2$	0.14	
	$(a_{1u})^1(b_{2g}/d_{xy})^2(a_{1g}/d_{z^2})^2(1e_g/d_\pi)^2$	0.78	
$[FePz]^{2+}$	$(a_{1u})^1(b_{2g}/d_{xy})^2(a_{1g}/d_{z^2})^1(1e_g/d_\pi)^2$	0	Fe^{III} (IP_2: 11.32)
	$(a_{1u})^2(b_{2g}/d_{xy})^1(a_{1g}/d_{z^2})^1(1e_g/d_\pi)^2$	0.10	
$[FePz]^{1-}$	$(b_{2g}/d_{xy})^2(a_{1g}/d_{z^2})^2(1e_g/d_\pi)^3$	0	Fe^{I}
	$(b_{2g}/d_{xy})^2(a_{1g}/d_{z^2})^2(1e_g/d_\pi)^3(2e_g)^1$	0.36	
$[FePz]^{2-}$	$(b_{2g}/d_{xy})^2(a_{1g}/d_{z^2})^2(1e_g/d_\pi)^4$	0	Fe^{0}
	$(b_{2g}/d_{xy})^2(a_{1g}/d_{z^2})^2(1e_g/d_\pi)^3(2e_g)^1$	0.35	
$[FePc]^{1+}$	$(b_{2g}/d_{xy})^2(a_{1u})^1(a_{1g}/d_{z^2})^2(1e_g/d_\pi)^2$	0	Fe^{II} (IP_1: 6.46)
	$(b_{2g}/d_{xy})^2(a_{1u})^2(a_{1g}/d_{z^2})^1(1e_g/d_\pi)^2$	0.04	
	$(b_{2g}/d_{xy})^1(a_{1u})^2(a_{1g}/d_{z^2})^2(1e_g/d_\pi)^2$	0.20	
$[FePc]^{2+}$	$(b_{2g}/d_{xy})^2(a_{1u})^1(a_{1g}/d_{z^2})^1(1e_g/d_\pi)^2$	0	Fe^{III} (IP_2: 9.39)
	$(b_{2g}/d_{xy})^2(a_{1u})^0(a_{1g}/d_{z^2})^2(1e_g/d_\pi)^2$	0.19	
	$(b_{2g}/d_{xy})^1(a_{1u})^1(a_{1g}/d_{z^2})^2(1e_g/d_\pi)^2$	0.23	
$[FePc]^{1-}$	$(b_{2g}/d_{xy})^2(a_{1g}/d_{z^2})^2(1e_g/d_\pi)^3$	0	Fe^{I}
	$(b_{2g}/d_{xy})^2(a_{1g}/d_{z^2})^2(1e_g/d_\pi)^2(2e_g)^1$	0.45	
$[FePc]^{2-}$	$(b_{2g}/d_{xy})^2(a_{1g}/d_{z^2})^2(1e_g/d_\pi)^4$	0	Fe^{0}
	$(b_{2g}/d_{xy})^2(a_{1g}/d_{z^2})^2(1e_g/d_\pi)^3(2e_g)^1$	0.55	
$[FePn]^{1+}$	$(a_{1u})^2(1a_{1g}/d_{xy})^2(2a_{1g}/d_{z^2})^1(1b_{3g}/d_{yz})^1(1b_{2g}/d_{xz})^1$	0	Fe^{III} (IP_1: 6.39)
	$(a_{1u})^2(1a_{1g}/d_{xy})^1(2a_{1g}/d_{z^2})^1(1b_{3g}/d_{yz})^2(1b_{2g}/d_{xz})^1$	0.43	
	$(a_{1u})^1(1a_{1g}/d_{xy})^2(2a_{1g}/d_{z^2})^1(1b_{3g}/d_{yz})^2(1b_{2g}/d_{xz})^1$	0.62	
$[FePn]^{2+}$	$(a_{1u})^1(1a_{1g}/d_{xy})^2(2a_{1g}/d_{z^2})^1(1b_{3g}/d_{yz})^1(1b_{2g}/d_{xz})^1$	0	Fe^{III} (IP_2: 10.58)
	$(a_{1u})^2(1a_{1g}/d_{xy})^1(2a_{1g}/d_{z^2})^1(1b_{3g}/d_{yz})^1(1b_{2g}/d_{xz})^1$	0.74	
$[FePn]^{1-}$	$(1a_{1g}/d_{xy})^2(2a_{1g}/d_{z^2})^1(1b_{3g}/d_{yz})^2(1b_{2g}/d_{xz})^2$	0	Fe^{I}
	$(1a_{1g}/d_{xy})^2(2a_{1g}/d_{z^2})^1(1b_{3g}/d_{yz})^2(1b_{2g}/d_{xz})^1(2b_{2g})^1$	0.01	
$[FePn]^{2-}$	$(1a_{1g}/d_{xy})^2(2a_{1g}/d_{z^2})^1(1b_{3g}/d_{yz})^2(1b_{2g}/d_{xz})^2(2b_{2g})^1$	0	Fe^{I}
	$(1a_{1g}/d_{xy})^2(2a_{1g}/d_{z^2})^2(1b_{3g}/d_{yz})^2(1b_{2g}/d_{xz})^2$	0.25	
$[FeDBPn]^{1+}$	$(b_{1u})^2(1a_{1g}/d_{xy})^2(2a_{1g}/d_{z^2})^1(1b_{2g}/d_{xz})^1(1b_{3g}/d_{yz})^1$	0	Fe^{III} (IP_1: 6.30)
	$(b_{1u})^2(1a_{1g}/d_{xy})^1(2a_{1g}/d_{z^2})^1(1b_{2g}/d_{xz})^2(1b_{3g}/d_{yz})^1$	0.43	
	$(b_{1u})^1(1a_{1g}/d_{xy})^2(2a_{1g}/d_{z^2})^1(1b_{2g}/d_{xz})^2(1b_{3g}/d_{yz})^1$	0.62	
$[FeDBPn]^{2+}$	$(b_{1u})^1(1a_{1g}/d_{xy})^2(2a_{1g}/d_{z^2})^1(1b_{2g}/d_{xz})^1(1b_{3g}/d_{yz})^1$	0	Fe^{III} (IP_2: 10.28)
	$(b_{1u})^2(1a_{1g}/d_{xy})^1(2a_{1g}/d_{z^2})^1(1b_{2g}/d_{xz})^1(1b_{3g}/d_{yz})^1$	0.33	
$[FeDBPn]^{1-}$	$(1a_{1g}/d_{xy})^2(2a_{1g}/d_{z^2})^1(1b_{2g}/d_{xz})^2(1b_{3g}/d_{yz})^1(2b_{2g})^1$	0	Fe^{II}
	$(1a_{1g}/d_{xy})^2(2a_{1g}/d_{z^2})^1(1b_{2g}/d_{xz})^2(1b_{3g}/d_{yz})^1$	0.09	
$[FeDBPn]^{2-}$	$(1a_{1g}/d_{xy})^2(2a_{1g}/d_{z^2})^2(1b_{2g}/d_{xz})^2(1b_{3g}/d_{yz})^1(2b_{2g})^1$	0	Fe^{I}
$[FeHPz]^{1+}$	$(b_{3g})^2(1b_{2g}/d_{xz})^2(1a_{1g}/d_{xy})^2(2a_{1g}/d_{z^2})^1(1b_{3g}/d_{yz})^0$	0	Fe^{III} (IP_1: 6.51)
	$(b_{3g})^2(1b_{2g}/d_{xz})^2(1a_{1g}/d_{xy})^1(2a_{1g}/d_{z^2})^1(1b_{3g}/d_{yz})^1$	0.04	
	$(b_{3g})^2(1b_{2g}/d_{xz})^1(1a_{1g}/d_{xy})^2(2a_{1g}/d_{z^2})^1(1b_{3g}/d_{yz})^1$	0.05	
	$(b_{3g})^1(1b_{2g}/d_{xz})^2(1a_{1g}/d_{xy})^2(2a_{1g}/d_{z^2})^1(1b_{3g}/d_{yz})^1$	0.26	
$[FeHPz]^{2+}$	$(b_{3g})^2(1b_{2g}/d_{xz})^1(1a_{1g}/d_{xy})^2(2a_{1g}/d_{z^2})^1(1b_{3g}/d_{yz})^0$	0	Fe^{IV} (IP_2: 9.92)
	$(b_{3g})^2(1b_{2g}/d_{xz})^2(1a_{1g}/d_{xy})^1(2a_{1g}/d_{z^2})^1(1b_{3g}/d_{yz})^0$	0.05	
	$(b_{3g})^1(1b_{2g}/d_{xz})^2(1a_{1g}/d_{xy})^2(2a_{1g}/d_{z^2})^1(1b_{3g}/d_{yz})^0$	0.24	
$[FeHPz]^{1-}$	$(1b_{2g}/d_{xz})^2(1a_{1g}/d_{xy})^2(2a_{1g}/d_{z^2})^2(1b_{3g}/d_{yz})^1$	0	Fe^{I}
	$(1b_{2g}/d_{xz})^2(1a_{1g}/d_{xy})^1(2a_{1g}/d_{z^2})^2(1b_{3g}/d_{yz})^1(2b_{2g})^1$	0.30	
$[FeHPz]^{2-}$	$(1b_{2g}/d_{xz})^2(1a_{1g}/d_{xy})^2(2a_{1g}/d_{z^2})^2(1b_{3g}/d_{yz})^1(2b_{2g})^1$	0	Fe^{I}
	$(1b_{2g}/d_{xz})^2(1a_{1g}/d_{xy})^2(2a_{1g}/d_{z^2})^2(1b_{3g}/d_{yz})^2$	0.34	
$[FeP(Py)_2]^{1+}$	$(b_{1u})^2(1b_{3g}/d_{yz})^2(1b_{2g}/d_{xz})^1(a_{1g}/d_{xy})^2$	0	Fe^{III} (IP_1: 5.67)
	$(b_{1u})^2(1b_{3g}/d_{yz})^1(1b_{2g}/d_{xz})^2(a_{1g}/d_{xy})^2$	0.03	
	$(b_{1u})^2(1b_{3g}/d_{yz})^2(1b_{2g}/d_{xz})^2(a_{1g}/d_{xy})^1$	0.24	
	$(b_{1u})^1(1b_{3g}/d_{yz})^2(1b_{2g}/d_{xz})^2(a_{1g}/d_{xy})^2$	0.67	
$[FeP(Py)_2]^{2+}$	$(b_{1u})^2(1b_{3g}/d_{yz})^1(1b_{2g}/d_{xz})^1(a_{1g}/d_{xy})^2$	0	Fe^{IV} (IP_2: 9.57)
	$(b_{1u})^1(1b_{3g}/d_{yz})^2(1b_{2g}/d_{xz})^1(a_{1g}/d_{xy})^2$	0.05	
	$(b_{1u})^2(1b_{3g}/d_{yz})^2(1b_{2g}/d_{xz})^1(a_{1g}/d_{xy})^1$	0.48	
$[FeP(Py)(CO)]^{1+}$	$(1a_1)^2(1b_2/d_{yz})^2(1b_1/d_{xz})^2(2a_1/d_{xy})^1$	0	Fe^{III} (IP_1: 6.53)
	$(1a_1)^2(1b_2/d_{yz})^2(1b_1/d_{xz})^1(2a_1/d_{xy})^2$	0.14	
	$(1a_1)^2(1b_2/d_{yz})^1(1b_1/d_{xz})^2(2a_1/d_{xy})^2$	0.15	
	$(1a_1)^1(1b_2/d_{yz})^2(1b_1/d_{xz})^2(2a_1/d_{xy})^2$	0.18	
$[FeP(Py)(CO)]^{2+}$	$(1a_1)^2(1b_2/d_{yz})^2(1b_1/d_{xz})^1(2a_1/d_{xy})^1$	0	Fe^{IV} (IP_2: 10.07)
	$(1a_1)^2(1b_2/d_{yz})^1(1b_1/d_{xz})^2(2a_1/d_{xy})^1$	0.00	
	$(1a_1)^1(1b_2/d_{yz})^2(1b_1/d_{xz})^2(2a_1/d_{xy})^1$	0.12	
$[FeP(CO)]^{1+}$	$(a_2)^1(1e/d_\pi)^4(b_2/d_{xy})^2$	0	Fe^{II} (IP_1: 7.05)
	$(a_2)^2(1e/d_\pi)^4(b_2/d_{xy})^1$	0.07	
	$(a_2)^2(1e/d_\pi)^3(b_2/d_{xy})^2$	0.10	

TABLE 6: Continued

system	configuration (see Figures 2−5)	E	oxidation state on Fe
$[FeP(CO)]^{2+}$	$(a_1)^2(a_2)^1(1e/d_\pi)^3(b_2/d_{xy})^2$	0	Fe^{III} (IP_2: 10.65)
	$(a_1)^2(a_2)^1(1e/d_\pi)^4(b_2/d_{xy})^1$	0.02	
	$(a_1)^1(a_2)^1(1e/d_\pi)^4(b_2/d_{xy})^2$	0.05	
$[FePz(Py)_2]^{1+}$	$(a_{1u})^2(1b_{3g}/d_{yz})^2(1b_{2g}/d_{xz})^1(a_{1g}/d_{xy})^2$	0	Fe^{III} (IP_1: 6.22)
	$(a_{1u})^2(1b_{3g}/d_{yz})^1(1b_{2g}/d_{xz})^2(a_{1g}/d_{xy})^2$	0.04	
	$(a_{1u})^2(1b_{3g}/d_{yz})^2(1b_{2g}/d_{xz})^2(a_{1g}/d_{xy})^1$	0.13	
	$(a_{1u})^1(1b_{3g}/d_{yz})^2(1b_{2g}/d_{xz})^2(a_{1g}/d_{xy})^2$	0.76	
$[FePz(Py)_2]^{2+}$	$(a_{1u})^2(1b_{3g}/d_{yz})^1(1b_{2g}/d_{xz})^1(a_{1g}/d_{xy})^2$	0	Fe^{IV} (IP_2: 10.02)
	$(a_{1u})^2(1b_{3g}/d_{yz})^2(1b_{2g}/d_{xz})^1(a_{1g}/d_{xy})^1$	0.19	
	$(a_{1u})^1(1b_{3g}/d_{yz})^2(1b_{2g}/d_{xz})^1(a_{1g}/d_{xy})^2$	0.36	
$[FePz(Py)(CO)]^{1+}$	$(a_2)^2(1b_2/d_{yz})^2(1b_1/d_{xz})^2(2a_1/d_{xy})^1$	0	Fe^{III} (IP_1: 7.00)
	$(a_2)^2(1b_2/d_{yz})^2(1b_1/d_{xz})^1(2a_1/d_{xy})^2$	0.13	
	$(a_2)^2(1b_2/d_{yz})^1(1b_1/d_{xz})^2(2a_1/d_{xy})^2$	0.14	
	$(a_2)^1(1b_2/d_{yz})^2(1b_1/d_{xz})^2(2a_1/d_{xy})^2$	0.35	
$[FePz(Py)(CO)]^{2+}$	$(a_2)^1(1b_2/d_{yz})^2(1b_1/d_{xz})^2(2a_1/d_{xy})^1$	0	Fe^{III} (IP_2: 10.88)
	$(a_2)^2(1b_2/d_{yz})^2(1b_1/d_{xz})^1(2a_1/d_{xy})^1$	0.09	
	$(a_2)^2(1b_2/d_{yz})^1(1b_1/d_{xz})^2(2a_1/d_{xy})^1$	0.10	
$[FePz(CO)]^{1+}$	$(a_2)^2(1e/d_\pi)^4(b_2/d_{xy})^1$	0	Fe^{III} (IP_1: 7.50)
	$(a_2)^1(1e/d_\pi)^4(b_2/d_{xy})^2$	0.20	
	$(a_2)^2(1e/d_\pi)^3(b_2/d_{xy})^2$	0.22	
$[FePz(CO)]^{2+}$	$(a_2)^1(1e/d_\pi)^4(b_2/d_{xy})^1$	0	Fe^{III} (IP_2: 11.37)
	$(a_2)^2(1e/d_\pi)^3(b_2/d_{xy})^1$	0.28	
$[FePc(Py)_2]^{1+}$	$(1b_{3g}/d_{yz})^2(a_{1u})^1(1b_{2g}/d_{xz})^2(a_{1g}/d_{xy})^2$	0	Fe^{II} (IP_1: 6.06)
	$(1b_{3g}/d_{yz})^2(a_{1u})^2(1b_{2g}/d_{xz})^1(a_{1g}/d_{xy})^2$	0.01	
	$(1b_{3g}/d_{yz})^1(a_{1u})^2(1b_{2g}/d_{xz})^2(a_{1g}/d_{xy})^2$	0.05	
	$(1b_{3g}/d_{yz})^2(a_{1u})^2(1b_{2g}/d_{xz})^2(a_{1g}/d_{xy})^1$	0.14	
$[FePc(Py)_2]^{2+}$	$(1b_{3g}/d_{yz})^2(a_{1u})^1(1b_{2g}/d_{xz})^1(a_{1g}/d_{xy})^2$	0	Fe^{III} (IP_2: 8.82)
	$(1b_{3g}/d_{yz})^1(a_{1u})^1(1b_{2g}/d_{xz})^2(a_{1g}/d_{xy})^2$	0.02	
	$(1b_{3g}/d_{yz})^2(a_{1u})^1(1b_{2g}/d_{xz})^2(a_{1g}/d_{xy})^1$	0.19	
	$(1b_{3g}/d_{yz})^2(a_{1u})^0(1b_{2g}/d_{xz})^2(a_{1g}/d_{xy})^2$	0.20	
$[FePc(Py)(CO)]^{1+}$	$(1b_2/d_{yz})^2(1b_1/d_{xz})^2(2a_1/d_{xy})^2(a_2)^1$	0	Fe^{II} (IP_1: 6.29)
	$(1b_2/d_{yz})^2(1b_1/d_{xz})^2(2a_1/d_{xy})^1(a_2)^2$	0.50	
	$(1b_2/d_{yz})^2(1b_1/d_{xz})^1(2a_1/d_{xy})^2(a_2)^2$	0.58	
	$(1b_2/d_{yz})^1(1b_1/d_{xz})^2(2a_1/d_{xy})^2(a_2)^2$	0.60	
$[FePc(Py)(CO)]^{2+}$	$(1b_2/d_{yz})^2(1b_1/d_{xz})^2(2a_1/d_{xy})^2(a_2)^0$	0	Fe^{II} (IP_2: 9.29)
	$(1b_2/d_{yz})^2(1b_1/d_{xz})^2(2a_1/d_{xy})^1(a_2)^1$	0.36	
	$(1b_2/d_{yz})^2(1b_1/d_{xz})^1(2a_1/d_{xy})^2(a_2)^1$	0.36	
	$(1b_2/d_{yz})^1(1b_1/d_{xz})^2(2a_1/d_{xy})^2(a_2)^1$	0.37	
$[FePc(CO)]^{1+}$	$(1e/d_\pi)^4(b_2/d_{xy})^2(a_2)^1$	0	Fe^{II} (IP_1: 6.51)
	$(1e/d_\pi)^4(b_2/d_{xy})^1(a_2)^2$	0.66	
	$(1e/d_\pi)^3(b_2/d_{xy})^2(a_2)^2$	0.77	
$[FePc(CO)]^{2+}$	$(1e/d_\pi)^4(b_2/d_{xy})^2(a_2)^0$	0	Fe^{II} (IP_2: 9.56)
	$(1e/d_\pi)^4(b_2/d_{xy})^1(a_2)^1$	0.54	
	$(1e/d_\pi)^3(b_2/d_{xy})^2(a_2)^1$	0.57	
$[FePn(Py)_2]^{1+}$	$(a_{1u})^2(1b_{3g}/d_{yz})^2(a_{1g}/d_{xy})^2(1b_{2g}/d_{xz})^1$	0	Fe^{III} (IP_1: 5.37)
	$(a_{1u})^2(1b_{3g}/d_{yz})^1(a_{1g}/d_{xy})^2(1b_{2g}/d_{xz})^2$	0.28	
	$(a_{1u})^2(1b_{3g}/d_{yz})^2(a_{1g}/d_{xy})^1(1b_{2g}/d_{xz})^2$	0.45	
	$(a_{1u})^1(1b_{3g}/d_{yz})^2(a_{1g}/d_{xy})^2(1b_{2g}/d_{xz})^2$	1.09	
$[FePn(Py)_2]^{2+}$	$(a_{1u})^2(1b_{3g}/d_{yz})^1(a_{1g}/d_{xy})^2(1b_{2g}/d_{xz})^1$	0	Fe^{IV} (IP_2: 9.61)
	$(a_{1u})^1(1b_{3g}/d_{yz})^2(a_{1g}/d_{xy})^2(1b_{2g}/d_{xz})^1$	0.12	
	$(a_{1u})^2(1b_{3g}/d_{yz})^2(a_{1g}/d_{xy})^1(1b_{2g}/d_{xz})^1$	0.53	
$[FePn(Py)(CO)]^{1+}$	$(a_2)^2(1b_2/d_{yz})^2(1b_1/d_{xz})^1(2a_1/d_{xy})^2$	0	Fe^{III} (IP_1: 6.45)
	$(a_2)^2(1b_2/d_{yz})^2(1b_1/d_{xz})^2(2a_1/d_{xy})^1$	0.15	
	$(a_2)^2(1b_2/d_{yz})^1(1b_1/d_{xz})^2(2a_1/d_{xy})^2$	0.21	
	$(a_2)^1(1b_2/d_{yz})^2(1b_1/d_{xz})^2(2a_1/d_{xy})^2$	0.33	
$[FePn(Py)(CO)]^{2+}$	$(a_2)^2(1b_2/d_{yz})^2(1b_1/d_{xz})^1(2a_1/d_{xy})^1$	0	Fe^{IV} (IP_2: 10.14)
	$(a_2)^1(1b_2/d_{yz})^2(1b_1/d_{xz})^1(2a_1/d_{xy})^2$	0.01	
	$(a_2)^2(1b_2/d_{yz})^1(1b_1/d_{xz})^1(2a_1/d_{xy})^2$	0.32	
$[FePn(CO)]^{1+}$	$(a_2)^2(1b_2/d_{yz})^2(1b_1/d_{xz})^2(2a_1/d_{xy})^1$	0	Fe^{III} (IP_1: 6.98)
	$(a_2)^2(1b_2/d_{yz})^2(1b_1/d_{xz})^1(2a_1/d_{xy})^2$	0.00	
	$(a_2)^1(1b_2/d_{yz})^2(1b_1/d_{xz})^2(2a_1/d_{xy})^2$	0.12	
	$(a_2)^2(1b_2/d_{yz})^1(1b_1/d_{xz})^2(2a_1/d_{xy})^2$	0.19	
$[FePn(CO)]^{2+}$	$(a_2)^2(1b_2/d_{yz})^2(1b_1/d_{xz})^1(2a_1/d_{xy})^1$	0	Fe^{IV} (IP_2: 10.61)
	$(a_2)^1(1b_2/d_{yz})^2(1b_1/d_{xz})^2(2a_1/d_{xy})^1$	0.03	
	$(a_2)^2(1b_2/d_{yz})^1(1b_1/d_{xz})^2(2a_1/d_{xy})^1$	0.17	
$[FeDBPn(Py)_2]^{1+}$	$(b_{1u})^2(1b_{2g}/d_{xz})^2(a_{1g}/d_{xy})^2(1b_{3g}/d_{yz})^1$	0	Fe^{III} (IP_1: 5.68)
	$(b_{1u})^2(1b_{2g}/d_{xz})^1(a_{1g}/d_{xy})^2(1b_{3g}/d_{yz})^2$	0.05	
	$(b_{1u})^2(1b_{2g}/d_{xz})^2(a_{1g}/d_{xy})^1(1b_{3g}/d_{yz})^2$	0.33	
	$(b_{1u})^1(1b_{2g}/d_{xz})^2(a_{1g}/d_{xy})^2(1b_{3g}/d_{yz})^2$	0.58	
$[FeDBPn(Py)_2]^{2+}$	$(b_{1u})^2(1b_{2g}/d_{xz})^1(a_{1g}/d_{xy})^2(1b_{3g}/d_{yz})^1$	0	Fe^{IV} (IP_2: 9.19)
	$(b_{1u})^1(1b_{2g}/d_{xz})^2(a_{1g}/d_{xy})^2(1b_{3g}/d_{yz})^1$	0.18	
	$(b_{1u})^2(1b_{2g}/d_{xz})^2(a_{1g}/d_{xy})^1(1b_{3g}/d_{yz})^1$	0.42	

TABLE 6: Continued

system	configuration (see Figures 2−5)	*E*	oxidation state on Fe
$[FeDBPn(Py)(CO)]^{1+}$	$(1a_1)^2(1b_1/d_{xz})^2(1b_2/d_{yz})^1(2a_1/d_{xy})^2$	0	Fe^{III} (IP_1: 6.32)
	$(1a_1)^2(1b_1/d_{xz})^2(1b_2/d_{yz})^2(2a_1/d_{xy})^1$	0.08	
	$(1a_1)^1(1b_1/d_{xz})^2(1b_2/d_{yz})^2(2a_1/d_{xy})^2$	0.20	
	$(1a_1)^2(1b_1/d_{xz})^1(1b_2/d_{yz})^2(2a_1/d_{xy})^2$	0.28	
$[FeDBPn(Py)(CO)]^{2+}$	$(1a_1)^2(1b_1/d_{xz})^2(1b_2/d_{yz})^1(2a_1/d_{xy})^1$	0	Fe^{IV} (IP_2: 9.73)
	$(1a_1)^2(1b_1/d_{xz})^1(1b_2/d_{yz})^1(2a_1/d_{xy})^2$	0.25	
	$(1a_1)^1(1b_1/d_{xz})^2(1b_2/d_{yz})^1(2a_1/d_{xy})^2$	0.36	
$[FeDBPn(CO)]^{1+}$	$(1a_1)^2(1b_1/d_{xz})^2(1b_2/d_{yz})^1(2a_1/d_{xy})^2$	0	Fe^{III} (IP_1: 6.68)
	$(1a_1)^2(1b_1/d_{xz})^2(1b_2/d_{yz})^2(2a_1/d_{xy})^1$	0.17	
	$(1a_1)^1(1b_1/d_{xz})^2(1b_2/d_{yz})^2(2a_1/d_{xy})^2$	0.32	
	$(1a_1)^2(1b_1/d_{xz})^1(1b_2/d_{yz})^2(2a_1/d_{xy})^2$	0.34	
$[FeDBPn(CO)]^{2+}$	$(1a_1)^2(1b_1/d_{xz})^2(1b_2/d_{yz})^1(2a_1/d_{xy})^1$	0	Fe^{IV} (IP_2: 10.30)
	$(1a_1)^2(1b_1/d_{xz})^1(1b_2/d_{yz})^1(2a_1/d_{xy})^2$	0.19	
	$(1a_1)^1(1b_1/d_{xz})^2(1b_2/d_{yz})^1(2a_1/d_{xy})^2$	0.24	
$[FeHPz(Py)_2]^{1+}$	$(b_{3g})^2(1b_{2g}/d_{xz})^2(a_{1g}/d_{xy})^2(1b_{3g}/d_{yz})^1$	0	Fe^{III} (IP_1: 5.48)
	$(b_{3g})^2(1b_{2g}/d_{xz})^2(a_{1g}/d_{xy})^1(1b_{3g}/d_{yz})^2$	0.61	
	$(b_{3g})^2(1b_{2g}/d_{xz})^1(a_{1g}/d_{xy})^2(1b_{3g}/d_{yz})^2$	0.74	
	$(b_{3g})^1(1b_{2g}/d_{xz})^2(a_{1g}/d_{xy})^2(1b_{3g}/d_{yz})^2$	0.88	
$[FeHPz(Py)_2]^{2+}$	$(b_{3g})^2(1b_{2g}/d_{xz})^2(a_{1g}/d_{xy})^2(1b_{3g}/d_{yz})^0$	0	Fe^{IV} (IP_2: 9.12)
	$(b_{3g})^1(1b_{2g}/d_{xz})^2(a_{1g}/d_{xy})^2(1b_{3g}/d_{yz})^1$	0.21	
	$(b_{3g})^2(1b_{2g}/d_{xz})^2(a_{1g}/d_{xy})^1(1b_{3g}/d_{yz})^1$	0.37	
	$(b_{3g})^2(1b_{2g}/d_{xz})^1(a_{1g}/d_{xy})^2(1b_{3g}/d_{yz})^1$	0.43	
$[FeHPz(Py)(CO)]^{1+}$	$(a_1/d_{xy})^2(1b_2)^1$	0	Fe^{II} (IP_1: 6.11)
	$(a_1/d_{xy})^1(1b_2)^2$	0.68	
$[FeHPz(Py)(CO)]^{2+}$	$(a_1/d_{xy})^2(1b_2)^0$	0	Fe^{II} (IP_2: 9.62)
	$(a_1/d_{xy})^1(1b_2)^1$	0.93	
$[FeHPz(CO)]^{1+}$	$(a_1/d_{xy})^2(1b_2)^1$	0	Fe^{II} (IP_1: 6.46)
	$(a_1/d_{xy})^1(1b_2)^2$	0.75	
$[FeHPz(CO)]^{2+}$	$(a_1/d_{xy})^2(1b_2)^0$	0	Fe^{II} (IP_2: 10.02)
	$(a_1/d_{xy})^1(1b_2)^1$	0.91	

[a] In parentheses, IP_1 = first ionization potential; IP_2 = second ionization potential. Units in eV.

TABLE A1: Calculated Properties of RuP(CO)

$R_{Ru-N(eq)}$ (Å)	$R_{Ru-C(ax)}$ (Å)	$R_{Ct\cdots Ru}$ (Å)	E_{bind} (eV) (RuP−CO)	Q_{Ru} (e)	IP[a] (eV) b_2/d_{xy}	IP[a] (eV) $1e/d_\pi$	IP[a] (eV) a_2	IP[a] (eV) a_1	EA[a] (eV)
2.066	1.796	0.124	2.64	1.32	7.54	7.23	7.10	7.11	−1.42 (2e)

[a] See Figure 3 [FeP(CO)] for the orbitals.

TABLE A2: Calculated Relative Energies (*E*, eV) for Selected Configurations in $[RuP(CO)]^+$ and $[RuP(CO)]^{2+}$ [a]

system	configuration[b]	*E*	oxidation state of Ru
$[RuP(CO)]^+$	$(a_2)^1(1e/d_\pi)^4(b_2/d_{xy})^2$	0	Ru^{II} (IP_1: 7.10)
	$(a_2)^2(1e/d_\pi)^3(b_2/d_{xy})^2$	0.13	
	$(a_2)^2(1e/d_\pi)^4(b_2/d_{xy})^1$	0.44	
$[RuP(CO)]^{2+}$	$(a_1)^1(a_2)^1(1e/d_\pi)^4(b_2/d_{xy})^2$	0	Ru^{II} (IP_2: 10.66)
	$(a_1)^2(a_2)^1(1e/d_\pi)^3(b_2/d_{xy})^2$	0.03	
	$(a_1)^2(a_2)^1(1e/d_\pi)^4(b_2/d_{xy})^1$	0.40	

[a] IP_1 = first ionization potential; IP_2 = second ionization potential. Units in eV. [b] See Figure 3 [FeP(CO)] for the orbitals.

properties different from the analogous Fe compounds.[56] It would be of interest to make a comparison of the ionization properties between FeP(CO) and RuP(CO). Therefore, additional calculations have been performed for the latter system and its ions. The results are presented in Tables A1 and A2.

The Ru−N(eq) and Ru−C(ax) bond lengths are about 0.1 Å larger than in the Fe analogue, but there is a smaller metal out-of-plane displacement in RuP(CO) than in FeP(CO). The value of E_{bind} indicates that CO is much more strongly bound to Ru than to Fe. The IP_1 and EA, which arise from the macrocycle orbitals, are shown to be little affected by the nature of the metal.

Similar to FeP(CO), the first ionization of RuP(CO) occurs from the a_2 (P−a_{1u}) orbital. Further ionization to yield $[RuP(CO)]^{2+}$ takes place from the a_1 orbital, which is also a macrocycle orbital. This is now in contrast to FeP(CO). In fact, as electrochemical studies have shown,[56] the RuP(Py)(CO) and FeP(Py)(CO) isomers also differ with regard to the site of oxidation. This experimental finding has been confirmed by the calculations performed by one of us.[57]

Acknowledgment. We thank Professor N. Shafizadeh of the University of Paris 11 for providing us with a copy of ref 49. The authors also gratefully acknowledge computational facilities provided by the Mississippi Supercomputer Center. This work is supported by the National Institutes of Health (S06 GM08047).

Supporting Information Available: ADF calculations on iron porphine (FeP) and a comparison of the results obtained from different computational methods. This material is available free of charge via the Internet at http://pubs.acs.org.

References and Notes

(1) (a) *The Porphyrins*; Dolphin, D., Ed.; Academic: New York, 1978; Vols. I−VII. (b) *Iron Porphyrin*; Lever, A. B. P., Gray, H. B., Eds.; Addison-Wesley Publishing Company, Inc.: Reading, MA, 1983.

(2) *Phthalocyanines: Properties and Applications*; Leznoff, C. C., Lever, A. B. P., Eds.; VCH Publishers: New York, 1989, 1993, 1996; Vols. 1− 4.

(3) Esposito, J. N.; Sutton, L. E.; Kenney, M. E. *Inorg. Chem.* **1967**, *6*, 1116.

(4) Attanasio, D.; Collamati, I.; Cervone, E. *Inorg. Chem.* **1983**, *22*, 3281.

(5) (a) Collamati, I.; Cervone, E.; Scoccia, R. *Inorg. Chim. Acta* **1985**, *98*, 11. (b) Dirk, C. W.; Mark, T. J. *Inorg. Chem.* **1984**, *23*, 4325. (c) Sakata, K.; Hayashi, Y.-I.; Gondo, K.; Mashimoto, M. *Inorg. Chim. Acta* **1989**, *156*, 1.

(6) Ofir, H.; Regev, A.; Levanon, H.; Vogel, E.; Köcher, M.; Balci, M. *J. Phys. Chem.* **1987**, *91*, 2686.
(7) Schlüpmann, J.; Huber, M.; Toporowicz, M.; Köcher, M.; Vogel, E.; Levanon, H.; Möbius, K. *J. Am. Chem. Soc.* **1988**, *110*, 8566.
(8) Levanon, H.; Toporowicz, M.; Ofir, H.; Fessenden, R. W.; Das, P. K.; Vogel, E.; Köcher, M.; Pramod, K. *J. Phys. Chem.* **1988**, *92*, 2429.
(9) Renner, M. W.; Forman, A.; Wu, W.; Chang, C. K.; Fajer, J. *J. Am. Chem. Soc.* **1989**, *111*, 8618.
(10) Gisselbrecht, J. P.; Gross, M.; Köcher, M.; Lausmann, M.; Vogel, E. *J. Am. Chem. Soc.* **1990**, *112*, 8618.
(11) D'Souza, F.; Boulas, P.; Aukauloo, A. M.; Guilard, R.; Kisters, M.; Vogel, E.; Kadish, K. M. *J. Phys. Chem.* **1994**, *98*, 11885.
(12) Bernard, C.; Gisselbrecht, J. P.; Gross, M.; Vogel, E.; Lausmann, M. *Inorg. Chem.* **1994**, *33*, 2393.
(13) Kadish, K. M.; D'Souza, F.; van Gaemelbecke, E.; Boulas, P.; Vogel, E.; Aukauloo, A. M.; Guilard, R. *Inorg. Chem.* **1994**, *33*, 4474.
(14) Bernard, C.; Gisselbrecht, J. P.; Gross, M.; Jux, N.; Vogel, E. *J. Electroanal. Chem.* **1995**, *381*, 159.
(15) D'Souza, F.; Boulas, P. L.; Kisters, M.; Sambrotta, L.; Aukauloo, A. M.; Guilard, R.; Kadish, K. M. *Inorg. Chem.* **1996**, *35*, 5743.
(16) Kadish, K. M.; Boulas, P. L.; Kisters, M.; Vogel, E.; Aukauloo, A. M.; D'Souza, F.; Guilard, R. *Inorg. Chem.* **1998**, *37*, 2693.
(17) Bernard, C.; LeMest, Y.; Giseelbrecht, J. P. *Inorg. Chem.* **1998**, *37*, 181.
(18) Gross, Z.; Simkhovich, L.; Galili, N. *Chem. Commun.* **1999**, 599.
(19) Shuali, Z.; Berg, A.; Levanon, H.; Vogel, E.; Bröring, M.; Sessler, J. L.; Fowler, C.; Weghorn, S. J. *Chem. Phys. Lett.* **1999**, *300*, 687.
(20) Gisselbrecht, J. P.; Gross, M.; Vogel, E.; Sessler, J. L. *Inorg. Chem.* **2000**, *39*, 2850.
(21) Gisselbrecht, J. P.; Gross, M.; Vogel, E.; Scholz, P.; Bröring, M.; Sessler, J. L. *J. Electroanal. Chem.* **2001**, *507*, 244.
(22) Ghosh, A.; Moulder, J.; Bröring, M.; Vogel, E. *Angew. Chem., Int. Ed.* **2001**, *40*, 431.
(23) Hayashi, T.; Okazaki, K.; Urakawa, N.; Shimakoshi, H.; Sessler, J. L.; Vogel, E.; Hisaeda, Y. *Organometallics* **2001**, *20*, 3074.
(24) Gorski, A.; Vogel, E.; Sessler, J. L.; Waluk, J. *J. Phys. Chem. A* **2002**, *106*, 8139.
(25) (a) Fowler, C. J.; Sessler, J. L.; Lynch, V. M.; Waluk, J.; Gebauer, A.; Lex, J.; Heger, A.; Zuniga-Rivero, F.; Vogel, E. *Chem.—Eur. J.* **2002**, *8*, 3485. (b) Rachlewicz, K.; Latos-Grażyński, L.; Vogel, E. *Inorg. Chem.* **2000**, *39*, 3247. (c) Rachlewicz, K.; Latos-Grażyński, L.; Vogel, E.; Ciunik, Z.; Jerzykiewicz, L. B. *Inorg. Chem.* **2002**, *41*, 1979.
(26) Gulam, R. M.; Matsushita, T.; Teraoka, J. *J. Phys. Chem. A* **2003**, *107*, 2172.
(27) Lang, G.; Spartalian, K.; Reed, C. A.; Collman, J. P. *J. Chem. Phys.* **1978**, *69*, 5424.
(28) Boyd, P. D. W.; Buckingham, A. D.; McMecking, R. F.; Mitra, S. *Inorg. Chem.* **1979**, *18*, 8,
(29) Liao, M.-S.; Scheiner, S. *J. Chem. Phys.* **2002**, *117*, 205.
(30) Liao, M.-S.; Scheiner, S. *J. Comput. Chem.* **2002**, *23*, 1391.
(31) Rosa, A.; Ricciardi, G.; Baerends, E. J.; van Gisbergen, S. J. A. *J. Phys. Chem. A* **2001**, *105*, 3311.
(32) Nguyen, K. A.; Pachter, R. *J. Chem. Phys.* **2001**, *114*, 10757−10767.
(33) Malsch, K.; Hohlneicher, G. *J. Phys. Chem. A* **1997**, *101*, 8409.
(34) Kozlowski, P. M.; Zgierski, M. Z.; Baker, J. *J. Chem. Phys.* **1998**, *109*, 5905.
(35) Waluk, J.; Müller, M.; Swiderek, P.; Köcher, M.; Vogel, E.; Hohlneicher, G.; Michl, J. *J. Am. Chem. Soc.* **1991**, *113*, 5511.
(36) Wu, Y.-D.; Chan, K. W. K. *THEOCHEM* **1997**, *398*−*399*, 325.
(37) (a) Bossa, M.; Cervone, E.; Garzillo, C.; Peluso, A. *THEOCHEM* **1997**, *390*, 101. (b) Bossa, M.; Cervone, E.; Garzillo, C.; DelRe, G. *THEOCHEM* **1995**, *242*, 73. (c) Bossa, M.; Grella, I.; Nota, P.; Cervone, E. *THEOCHEM* **1990**, *210*, 267.
(38) (a) Baerends, E. J.; Ellis, D. E.; Ros, P. *Chem. Phys.* **1973**, *2*, 41. (b) te Velde, G.; Baerends, E. J. *J. Comput. Phys.* **1992**, *99*, 84.
(39) Vosko, S. H.; Wilk, L.; Nusair, M. *Can. J. Phys.* **1980**, *58*, 1200.
(40) Becke, A. D. *Phys. Rev. A* **1988**, *38*, 3098.
(41) Perdew, J. P. *Phys. Rev. B* **1986**, *33*, 8822.
(42) Ziegler, T.; Tschinke, V.; Baerends, E. J.; Snijders, J. G.; Ravenek, W. *J. Phys. Chem.* **1989**, *93*, 3050.
(43) Stillman, M. J.; Thomson, A. J. *J. Chem. Soc., Faraday Trans. 2* **1974**, *70*, 790.
(44) Liao, M.-S.; Scheiner, S. *Chem. Phys. Lett.* **2003**, *367*, 199.
(45) Collman, J. P.; Hoard, J. L.; Kim, N.; Lang, G.; Reed, C. A. *J. Am. Chem. Soc.* **1975**, *97*, 2676.
(46) Kirner, J. F.; Dow, W.; Scheidt, W. R. *Inorg. Chem.* **1976**, *15*, 1685.
(47) Fitzgerald, J. P.; Haggerty, B. S.; Rheingold, A. L.; May, L.; Brewer, G. A. *Inorg. Chem.* **1992**, *31*, 2006.
(48) Shafizadeh, N.; Krim, L.; Sorgues, S.; Boep, B. *Chem. Phys. Lett.* **2002**, *357*, 37.
(49) Shafizadeh, N.; Sorgues, S.; Soep, B. *Chem. Phys. Lett.* **2004**, *391*, 380.
(50) (a) Rovira, C.; Kunc, K.; Hutter, J.; Ballone, P.; Parrinello, M. *J. Phys. Chem. A* **1997**, *101*, 8914. (b) Han, S.; Cho, K.; Ihm, J. *Phys. Rev. E* **1999**, *59*, 2218. (c) Ghosh, A.; Bocian, D. F. *J. Phys. Chem.* **1996**, *100*, 6363.
(51) Brown, G. M.; Hopf, F. R.; Ferguson, J. A.; Meyer, T. J.; Whitten, D. G. *J. Am. Chem. Soc.* **1973**, *95*, 5939.
(52) Peng, S. M.; Ibers, J. A. *J. Am. Chem. Soc.* **1976**, *98*, 8032.
(53) Lever, A. B. P.; Wilshire, J. P. *Inorg. Chem.* **1978**, *17*, 1145.
(54) Cocolios, P.; Kadish, K. M. *Isr. J. Chem.* **1985**, *25*, 138.
(55) Minor, P. C.; Gouterman, M.; Lever, A. B. P. *Inorg. Chem.* **1985**, *24*, 1894.
(56) Brown, G. M.; Hopf, F. R.; Meyer, T. J.; Whitten, D. G. *J. Am. Chem. Soc.* **1975**, *97*, 5385.
(57) Liao, M.-S.; Scheiner, S. *Chem. Phys.* **2002**, *285*, 195.